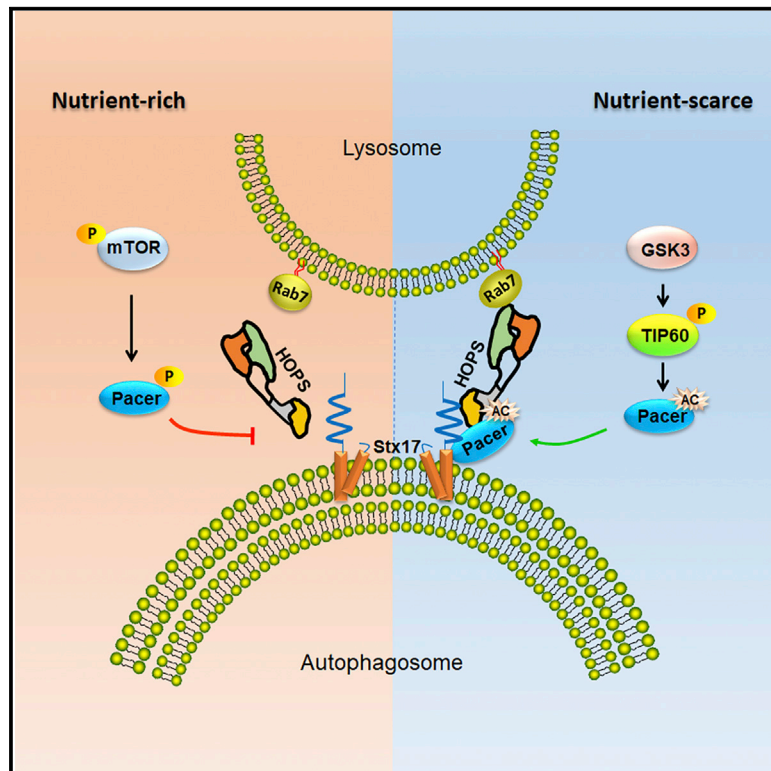


Molecular Cell

Pacer Is a Mediator of mTORC1 and GSK3-TIP60 Signaling in Regulation of Autophagosome Maturation and Lipid Metabolism

Graphical Abstract



Authors

Xiawei Cheng, Xiuling Ma, Qi Zhu, ..., Weihua Gong, Wei Liu, Qiming Sun

Correspondence

qmsun@zju.edu.cn

In Brief

Cheng et al. demonstrate that Pacer is essential for hepatic autophagy and liver homeostasis. Under autophagy induction conditions, mTORC1-mediated Pacer phosphorylation is repressed, which enables Pacer acetylation by the GSK3-TIP60 pathway. Pacer acetylation appears to be crucial for autolysosome formation and autophagic lipolysis.

Highlights

- Pacer is a regulator of hepatic autophagy and liver homeostasis
- Pacer is directly phosphorylated by mTORC1 under nutrient-rich conditions
- Dephosphorylated Pacer is acetylated by the GSK3-TIP60 pathway
- Pacer acetylation promotes autophagosome maturation and lipid metabolism

Pacer Is a Mediator of mTORC1 and GSK3-TIP60 Signaling in Regulation of Autophagosome Maturation and Lipid Metabolism

Xiawei Cheng,^{1,2} Xiuling Ma,^{1,2} Qi Zhu,^{1,2} Dandan Song,^{1,2} Xianming Ding,^{1,2} Lin Li,³ Xiao Jiang,^{1,2} Xinyi Wang,^{1,2} Rui Tian,^{1,2} Hua Su,^{1,2} Zhirong Shen,³ She Chen,³ Ting Liu,^{4,5} Weihua Gong,⁶ Wei Liu,^{1,2} and Qiming Sun^{1,2,7,*}

¹Department of Biochemistry, Second Affiliated Hospital, Zhejiang University School of Medicine, Hangzhou 310058, China

²Department of Cardiology, Second Affiliated Hospital, Zhejiang University School of Medicine, Hangzhou 310058, China

³National Institute of Biological Sciences, Beijing 102206, China

⁴Department of Cell Biology, Sir Run Run Shaw Hospital, Zhejiang University School of Medicine, Hangzhou 310058, China

⁵Department of General Surgery, Sir Run Run Shaw Hospital, Zhejiang University School of Medicine, Hangzhou 310058, China

⁶Department of Surgery, Second Affiliated Hospital, Zhejiang University School of Medicine, Hangzhou 310012, China

⁷Lead Contact

*Correspondence: qmsun@zju.edu.cn

<https://doi.org/10.1016/j.molcel.2018.12.017>

SUMMARY

mTORC1 and GSK3 play critical roles in early stages of (macro)autophagy, but how they regulate late steps of autophagy remains poorly understood. Here we show that mTORC1 and GSK3-TIP60 signaling converge to modulate autophagosome maturation through Pacer, an autophagy regulator that was identified in our recent study. Hepatocyte-specific Pacer knockout in mice results in impaired autophagy flux, glycogen and lipid accumulation, and liver fibrosis. Under nutrient-rich conditions, mTORC1 phosphorylates Pacer at serine157 to disrupt the association of Pacer with Stx17 and the HOPS complex and thus abolishes Pacer-mediated autophagosome maturation. Importantly, dephosphorylation of Pacer under nutrient-deprived conditions promotes TIP60-mediated Pacer acetylation, which facilitates HOPS complex recruitment and is required for autophagosome maturation and lipid droplet clearance. This work not only identifies Pacer as a regulator in hepatic autophagy and liver homeostasis *in vivo* but also reveals a signal integration mechanism involved in late stages of autophagy and lipid metabolism.

Q1 Q2 INTRODUCTION

Autophagy is an evolutionarily conserved process involving lysosomal degradation of cytoplasmic components, including proteins, glycogen, and lipids (Ktistakis and Tooze, 2016; Mizushima et al., 2011). Dysfunction of autophagy is implicated in a variety of human diseases (Mizushima et al., 2008; Rubinsztein et al., 2012). In mammalian cells, autophagy is initiated by biogenesis of isolation membranes, which then nucleate,

expand, and ultimately seal to form double membrane structures called autophagosome. Subsequently, autophagosomes fuse with lysosomes or late endosomes to form autolysosomes in a process called autophagosome maturation (Klionsky et al., 2016). Autophagy plays essential roles in maintaining cellular and organismal homeostasis by sensing nutrient, energy, and stress status (Kaur and Debnath, 2015; Kroemer et al., 2010). The currently known upstream regulations mainly work through early steps in autophagosome formation; however, it is not well understood how environmental stimuli are transduced to regulate autophagosome maturation, despite the remarkable progress that has recently been made in this area (Guo et al., 2014; Kim et al., 2015; Sun et al., 2015).

One of the crucial upstream mechanisms that regulate autophagy is the mTOR pathway (Ben-Sahra and Manning, 2017; He and Klionsky, 2009; Kroemer et al., 2010; Ktistakis and Tooze, 2016; Saxton and Sabatini, 2017). Under nutrient-rich conditions, mTOR complex 1 (mTORC1) inhibits early steps of autophagy by phosphorylating several autophagy core machineries, including Unc51-like kinase 1 (ULK1) and Atg13 (Chang and Neufeld, 2009; Ganley et al., 2009; Hosokawa et al., 2009; Jung et al., 2009; Kim et al., 2011), Atg14(L) and NRB2 (Ma et al., 2017; Yuan et al., 2013), autophagy/beclin-1 regulator 1 (Ambra1) (Nazio et al., 2013), and WIPI2 (Wan et al., 2018). Notably, the interplay of mTORC1 and AMPK is also crucial for of autophagy initiation by fine-tuning of ULK1 function (Egan et al., 2011; Kim et al., 2011; Mack et al., 2012; Shang and Wang, 2011). In addition, mTORC1 also indirectly regulates global autophagy flux by phosphorylating the transcription factor EB (TFEB) (Martina et al., 2012; Rocznik-Ferguson et al., 2012; Settembre et al., 2012). Recently, the critical function of mTOR pathway in late stages of autophagy began to emerge with the finding that mTOR terminates autophagy and drives autophagic lysosome reformation (Munson et al., 2015; Yu et al., 2010) and that mTORC1 targets UVRAG to inhibit autophagosome maturation (Kim et al., 2015). However, it remains unclear whether mTORC1 directly regulates other key factors involved in late stages of autophagy as well.

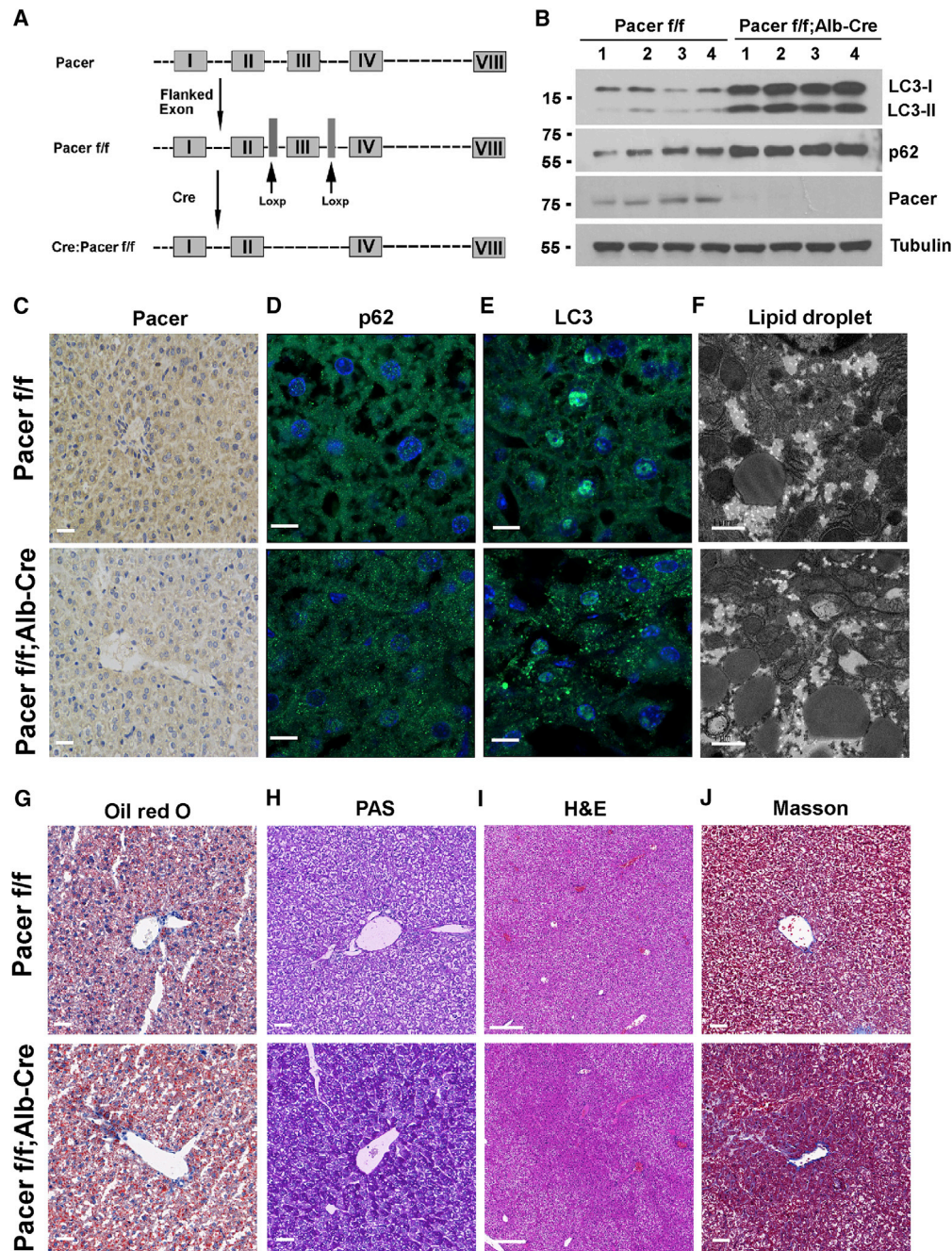


Figure 1. Pacer Is Important for Liver Autophagy and Lipid Homeostasis

(A) Schematic representation of the generation of conditional knockout mice of Pacer.

(B) The protein levels of the autophagy markers p62 and LC3 in the livers of four pairs of Pacer *f/f* and Pacer *f/f*; Alb-Cre mice for 8 weeks were determined by western blot.

(C) Immunohistochemistry showing Pacer protein expression in liver tissues of 8-week-old Pacer *f/f* and Pacer *f/f*; Alb-Cre mice. Scale bars, 100 μ m. 200 \times , n = 6.

(D) Immunofluorescence showing p62 protein levels in liver tissues of 8-week-old Pacer *f/f* and Pacer *f/f*; Alb-Cre mice. Scale bars, 50 μ m. 600 \times , n = 6.

(E) Immunofluorescence showing LC3 puncta in liver tissues of 8-week-old Pacer *f/f* and Pacer *f/f*; Alb-Cre mice. Scale bars, 50 μ m. 600 \times , n = 6.

(F) Transmission electron microscopy showing lipid droplets in liver tissues of 8-week-old Pacer *f/f* and Pacer *f/f*; Alb-Cre mice. Scale bars, 1 μ m. 8,300 \times , n = 6.

(G) Oil red O staining showing lipid accumulation in liver tissues of 8-week-old Pacer *f/f* and Pacer *f/f*; Alb-Cre mice. Scale bars, 100 μ m. 200 \times , n = 6.

(H) Periodic Acid-Schiff staining showing hepatic glycogen in liver tissues of 8-week-old Pacer *f/f* and Pacer *f/f*; Alb-Cre mice. Scale bars, 100 μ m. 200 \times , n = 6.

(I) H&E staining showing liver histopathologic changes in liver tissues of 8-week-old Pacer *f/f* and Pacer *f/f*; Alb-Cre mice. Scale bars, 100 μ m. 70 \times , n = 6.

(J) Masson staining showing liver fibrosis of 8-week-old Pacer *f/f* and Pacer *f/f*; Alb-Cre mice. Scale bars, 100 μ m. 200 \times , n = 6.

See also [Figure S1](#).

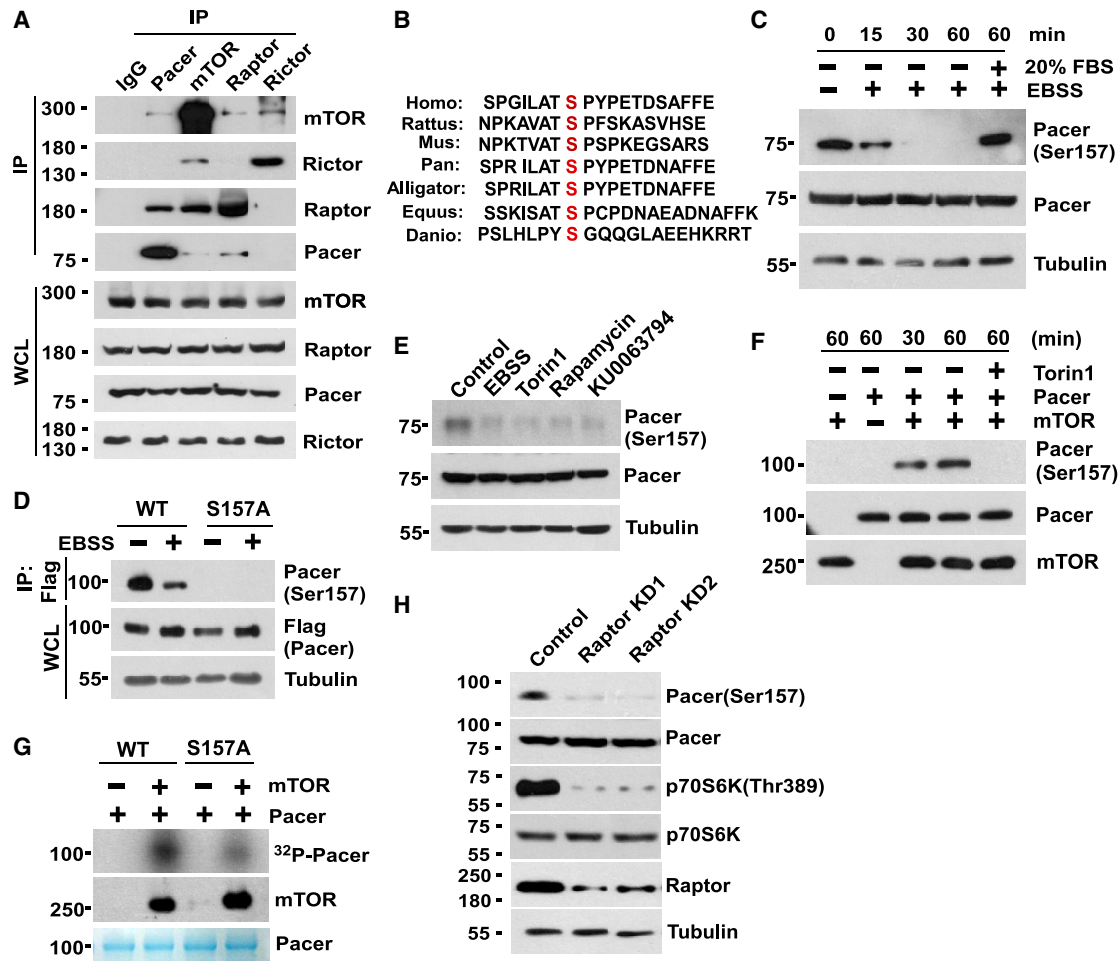


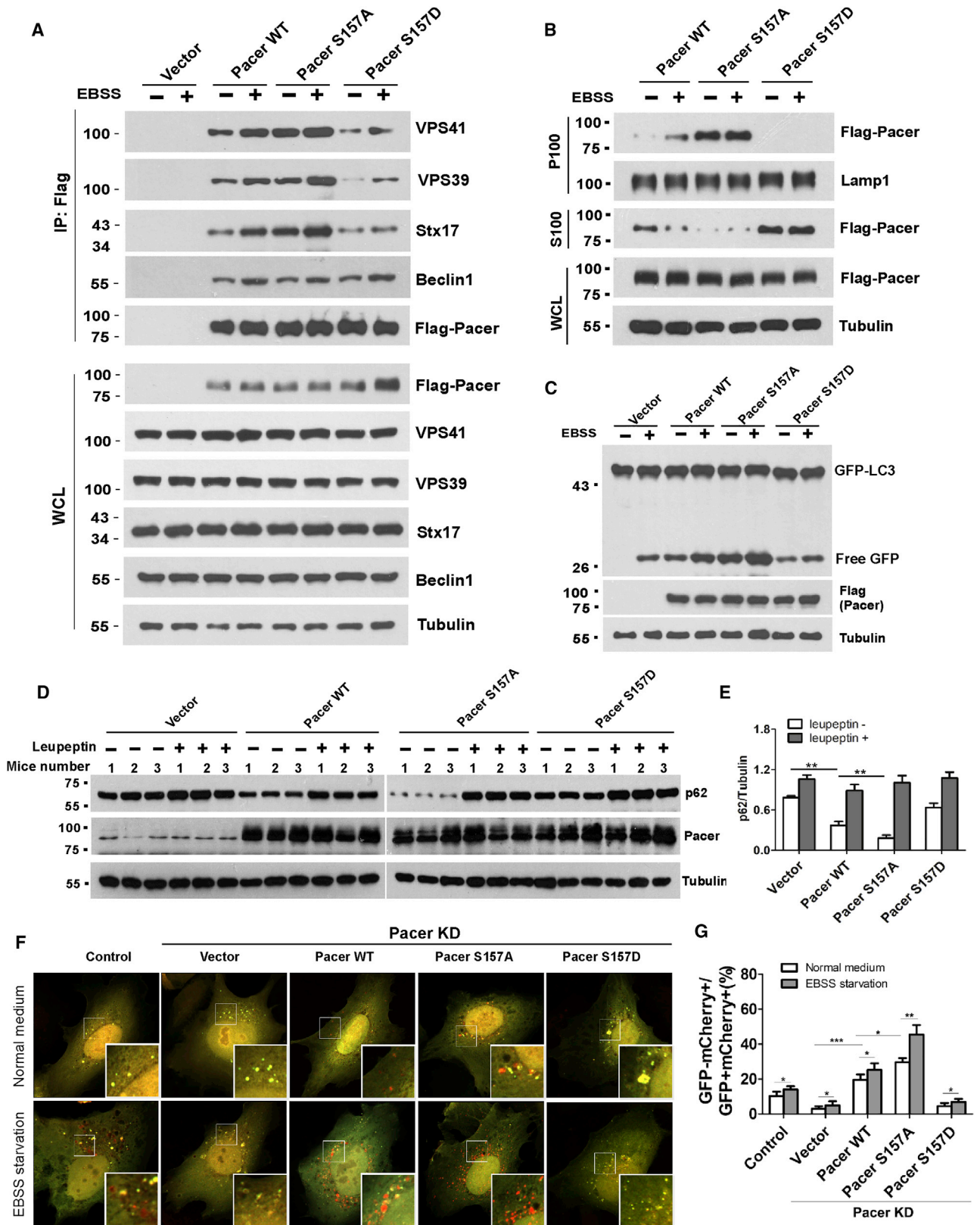
Figure 2. Serine157 of Pacer Is Phosphorylated by mTORC1 under Nutrient-Rich Conditions

(A) Pacer interacts with mTOR and Raptor. Endogenous Pacer, mTOR, Raptor, and Rictor were immunoprecipitated from HEK293T cells to analyze their interaction by western blot.
 (B) Alignment of primary sequences of Pacer from various species. Red indicates the identified phosphorylation site of Pacer.
 (C) The dynamic phosphorylation of Pacer at S157 in response to nutrient status. HEK293T cells were treated with EBSS (Earle's balanced salt solution) for 15, 30, and 60 min or cultured in complete medium for 2 h after 1 h of starvation. S157 phosphorylation levels were analyzed by phospho-Pacer(S157) antibody.
 (D) Antibody specificity test. Pacer^{WT}-FLAG and Pacer^{S157A}-FLAG HEK293T stable cell lines were cultured in complete medium or starved for 1 h. Immunoprecipitation was performed with anti-FLAG beads, and Pacer S157 phosphorylation levels were detected by western blot with phospho-Pacer S157 antibody.
 (E) Pacer S157 phosphorylation in HEK293T cells that were incubated with mTOR inhibitors (EBSS, Torin1, rapamycin, and KU0063794).
 (F) Pacer S157 phosphorylation assay *in vitro*. Endogenous mTOR was purified by immunoprecipitation (IP) from HEK293T cells, and its kinase activity *in vitro* was analyzed using purified Pacer^{WT}-FLAG as substrate at different time points. Torin1 was added to inhibit mTOR activity as a negative control.
 (G) Autoradiography of Pacer S157 phosphorylation *in vitro*. Recombinant Pacer^{WT}-FLAG and Pacer^{S157A}-FLAG proteins that were purified from *E. coli* were incubated with purified mTOR in kinase buffer containing γ -³²P-ATP. Pacer phosphorylation (³²P-Pacer) was analyzed by autoradiography.
 (H) Pacer S157 phosphorylation in Raptor KD HEK293T cells. HEK293T cells were transfected with Raptor shRNA for 72 h. Pacer S157 phosphorylation levels were detected by western blot.
 See also [Figure S2](#).

Under stressed conditions, mTORC1 activity is repressed in part by AMPK and GSK3, which phosphorylates and activates TSC2, a key inhibitory component of the mTOR pathway (Buller et al., 2008; Shin et al., 2011). In addition to its function in triggering autophagy through suppression of mTORC1 activity, GSK3 also phosphorylates and activates TIP60 or KAT5, a histone acetyltransferase, which subsequently acetylates and activates ULK1 to initiate autophagy (Lin et al., 2012; Nie et al., 2016). This regulation appears to be partially evolution-

arily conserved (Hamaï and Codogno, 2012; Yi et al., 2012) because Esa1p, the yeast homolog of TIP60, acetylates Atg3 to enhance the interaction between Atg3 and Atg8, which is a key step for Atg8 lipidation and subsequent autophagosome elongation (Yi et al., 2012). However, it is not known whether the GSK3-TIP60 pathway also regulates autophagosome maturation.

In our previous study, we identified a vertebrate-specific autophagy regulator, Pacer (Cheng et al., 2017), and showed that



(legend on next page)

Pacer facilitates the biogenesis of PI3P on autophagosomes. In addition, Pacer cooperates with Stx17 in recruitment of the HOPS complex to autophagosomes. Here we report that Pacer serves as a mediator of the convergent regulation of mTORC1 and GSK3-TIP60 signaling in autophagosome maturation and lipid metabolism both *in vitro* and *in vivo*.

RESULTS

Pacer Is Required for Hepatic Autophagy and Liver Homeostasis

To investigate Pacer's physiological function *in vivo*, we generated a liver-specific conditional knockout mouse model for Pacer by crossing mice carrying the floxed Pacer allele (Pacer *f/f*) with Alb-Cre mice (Figures 1A and S1A). Backcrossing of Pacer *f/+*; Alb-Cre mice led to homozygous ablation of Pacer in the mouse liver (Pacer *f/f*; Alb-Cre). Genotyping by PCR confirmed the presence of LoxP and Alb-Cre in mice (Figures S1B and S1C). An *in situ* hybridization assay verified the deletion of the LoxP-flanked region of *Pacer* genomic DNA in mouse hepatocytes (Figure S1D). Immunohistochemistry and western blot analysis further confirmed the depletion of Pacer expression (Figures 1B and 1C). Consistently, p62 and LC3 accumulated in (Pacer *f/f*; Alb-Cre) mice compared with the wild-type control mice (Pacer *f/f*) (Figures 1B, 1D, 1E, and S1E), which were similar to the phenotypes in Atg5 and Atg7 knockout mice (Komatsu et al., 2007; Toshima et al., 2014). The result indicated that Pacer deficiency hampered autophagosome maturation *in vivo*. A transmission electron microscope assay showed autophagosomes surrounding lipid droplets accumulated in Pacer-deficient hepatocytes (Figures 1F and S1F). In addition, Pacer depletion resulted in significant accumulation of lipid (Figures 1F, 1G, and S1G) and glycogen (Figure 1H) in hepatocytes, phenocopying Atg5 and Atg7 (Karsli-Uzunbas et al., 2014; Martinez-Lopez and Singh, 2015; Singh et al., 2009). Thus, Pacer regulates lipid and glycogen homeostasis in the liver. Remarkably, Pacer ablation resulted in collagen deposition (Figures 1I and 1J), a symptom of liver fibrosis, suggesting that Pacer deficiency causes liver damage. However, severe hepatomegaly and tumorigenesis (Komatsu et al., 2005; Takamura et al., 2011) were not observed in Pacer-deficient mouse livers during a

period of 4 months after birth. Although there was no significant difference in body weight between the wild-type and mutant mice (Figure S1H), Pacer knockout mice exhibited an increase in the ratio of liver to body weight (Figure S1I). Pacer knockout mice exhibited significantly lower total ketone bodies in the serum and liver after 24 h of fasting when compared with the wild-type control mice (Figures S1J and S1K). Together, these data indicate that Pacer maintains liver homeostasis and that it is an autophagy regulator in the liver.

mTORC1 Phosphorylates Pacer at S157 under Nutrient-Rich Conditions

It is currently still unknown whether Pacer is regulated by upstream signals. We obtained a clue regarding this question from our previous study (Cheng et al., 2017), in which mass spectrometry analysis of Pacer-coimmunoprecipitated proteins or protein complexes uncovered mLST8, a component of mTORC1 and mTORC2 (Ben-Sahra and Manning, 2017; Saxton and Sabatini, 2017), as a potential binding partner of Pacer (Figure S2A). Indeed, Pacer interacted with both endogenous and exogenous mTORC1 (Figures 2A, S2B, and S2C). Because Pacer overexpression (OE) was not able to affect mTOR signaling (Figure S2D), Pacer might be a new substrate of mTORC1. Mass spectrometry analysis identified the candidate phosphorylation site of Pacer to be serine157 (S157), which is positioned with a +1 proline (P), a preferred arrangement for mTOR recognition (Hsu et al., 2011). In addition, Pacer S157 is conserved across species ranging from zebrafish to humans (Figure 2B), implying an evolutionarily conserved regulatory mechanism. Using a phospho-specific antibody against human Pacer S157, we found that starvation reduced Pacer S157 phosphorylation, whereas re-feeding the cells with complete medium containing 20% fetal bovine serum (FBS) fully recovered Pacer S157 phosphorylation levels (Figure 2C). In addition, mutating S157 to alanine (S157A) completely abolished its phosphorylation (Figure 2D). Furthermore, mTOR inhibitors suppressed S157 phosphorylation in a manner similar to starvation (Figure 2E), and mTOR was able to phosphorylate Pacer at S157 *in vitro* (Figures 2F and 2G). Importantly, silencing Raptor, a component of mTORC1, but not Rictor, a subunit of mTORC2, impaired

Figure 3. Pacer S157 Phosphorylation Impairs Pacer Function in Autophagosome Maturation

- (A) S157 phosphorylation negatively regulates the Pacer-Stx17/HOPS interaction. FLAG-tagged Pacer^{WT}, Pacer^{S157A}, or Pacer^{S157D} were expressed individually in HEK293T cells that were treated without/with EBSS for 1 h. IP was performed using anti-FLAG beads, and samples were immunoblotted for endogenous Stx17, VPS39, VPS41, and Beclin1.
- (B) Subcellular localization assay by fractionation. HEK293T cells were transfected with FLAG-tagged Pacer^{WT}, Pacer^{S157A}, or Pacer^{S157D} and then treated without/with EBSS for 1 h. Then cell lysates were prepared and separated into P100 (precipitate) and S100 (supernatant) by ultracentrifugation, followed by western blot.
- (C) GFP-LC3 cleavage assay. HEK293T stable cell lines harboring GFP-LC3 vector were transfected with vector, FLAG-tagged Pacer^{WT}, Pacer^{S157A}, or Pacer^{S157D}. Shown is a western blot for the free GFP fragment using anti-GFP antibody.
- (D) Autophagy flux assay in mouse livers. Mice were intraperitoneally injected with HA-tagged rAAV-Pacer^{WT}, Pacer^{S157A}, or Pacer^{S157D} and treated with or without 40 mg/kg leupeptin for 12 h. Liver autophagy levels were analyzed by p62 degradation using western blot.
- (E) Statistical analysis of p62 in (D). Data are shown as mean \pm SD; **p < 0.01, n = 3.
- (F) Autophagosome maturation assay in U2OS cells. mCherry-GFP-LC3 was expressed in U2OS cells (control shRNA, Pacer KD/rescued by vector, Pacer^{WT}, Pacer^{S157A}, or Pacer^{S157D}) and analyzed by confocal microscopy. Only merged images are shown.
- (G) Quantification of the relative GFP⁺mCherry⁺ LC3 puncta as indicators of autophagosome maturation. For quantification, at least 60 cells were counted for each pair of colocalization analyses. Data are shown as mean \pm SD; *p < 0.05, ***p < 0.001, n = 60.
- See also Figure S3.

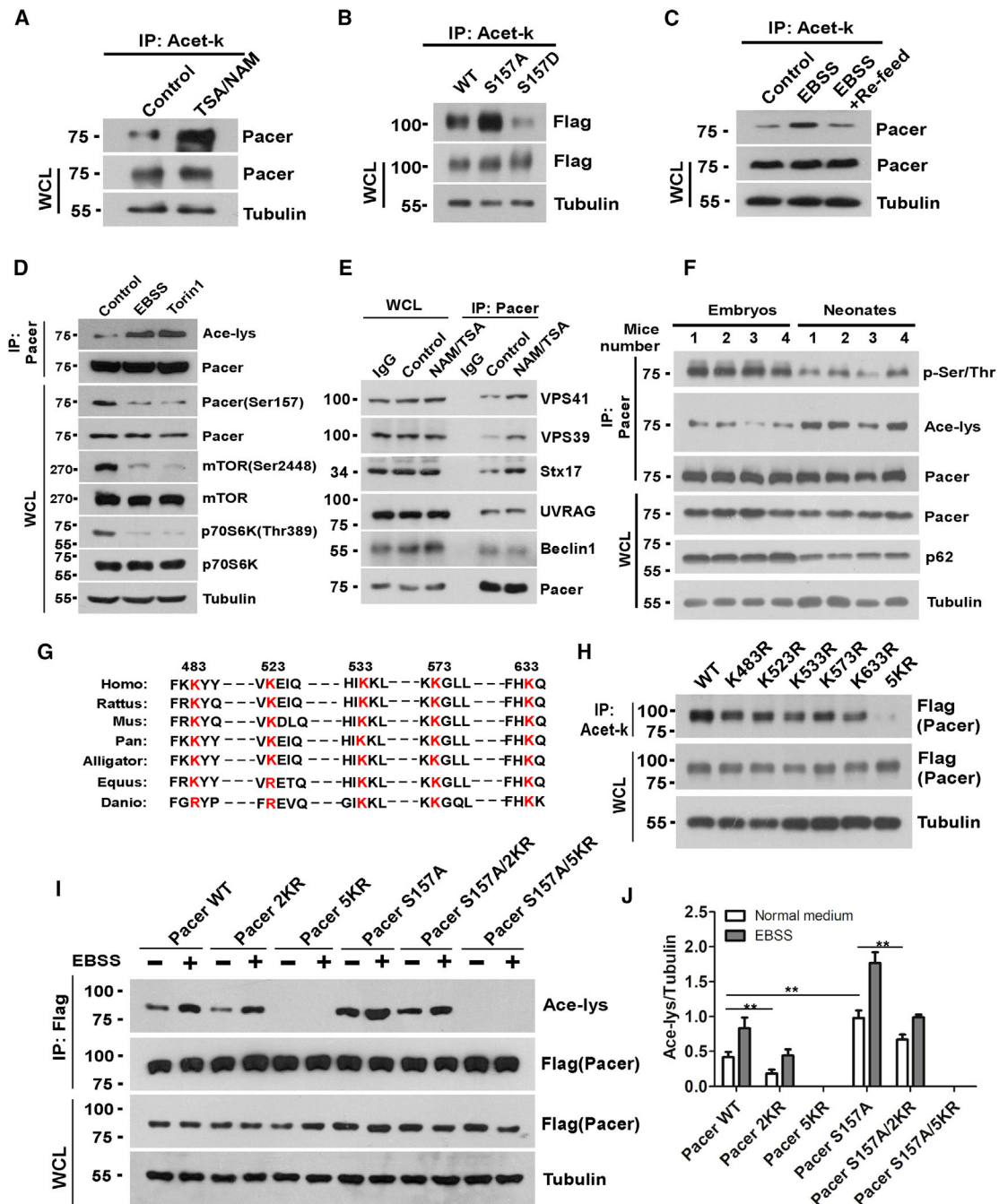


Figure 4. Pacer Ser157 Phosphorylation Regulates Pacer Acetylation at Its C-Terminal RH Domain

(A) Acetylation of endogenous Pacer in HEK293T cells. Cells were treated with or without the HDAC inhibitor trichostatin (TSA) (1 mM) and Sirtuin inhibitor nicotinamide (NAM) (5 mM) for 12 h. IP was performed with an antibody to acetylated lysine and western blot with an antibody to Pacer.

(B) Acetylation assay of Pacer S157 mutants in HEK293T cells transfected with FLAG-tagged Pacer^{WT}, Pacer^{S157A}, or Pacer^{S157D}. Acetylation assay methods were as in (A).

(C) Acetylation assay of endogenous Pacer under starvation conditions. HEK293T cells were starved or cultured in complete medium for 2 h after starvation for 1 h. Acetylation assay methods were as in (A).

(D) Acetylation assay of endogenous Pacer under mTORC1 inhibition. HEK293T cells were treated with EBSS for 1 h or with Torin1 (250 nM) for 2 h. IP was performed with a Pacer antibody and western blot with an antibody to acetylated lysine.

(E) The association of Pacer with known interactors in the presence of HDAC and Sirtuin inhibitors. HEK293T cells were treated with or without the HDAC inhibitor TSA (1 mM) and the Sirtuin inhibitor NAM (5 mM) for 12 h. IP was performed with an antibody to Pacer and western blot with an antibody to proteins, as indicated.

(legend continued on next page)

S157 phosphorylation (Figures 2H and S2E). Together, these results show that mTORC1 directly phosphorylates Pacer at S157 under nutrient-rich conditions.

Pacer S157 Phosphorylation Impairs Pacer Function in Autophagosome Maturation

To associate with autophagosomes, Pacer directly binds to autophagosomal Stx17 through its N-terminal region (Pacer^{100–200aa}) (Cheng et al., 2017). Therefore, it is possible that Pacer S157 phosphorylation may affect its interaction with Stx17. Indeed, Pacer^{S157A}, a mutant that mimics permanent de-phosphorylation, pulled down more endogenous Stx17 compared with wild-type Pacer (Pacer^{WT}) (Figure 3A). In contrast, the permanent phosphorylation mutant Pacer^{S157D} co-immunoprecipitated with reduced levels of Stx17. Unexpectedly, Pacer S157 phosphorylation also hampered its interaction with the HOPS complex (Figure 3A). Furthermore, starvation stress further increased the association of Pacer^{WT}, Pacer^{S157A}, or, to a less extent, Pacer^{S157D} with the indicated known binding partners. Indeed, Pacer S157 phosphorylation impeded its autophagosome targeting, which was verified by membrane fractionation assay and confocal microscopy analysis (Figures 3B, S3A, and S3B). Consequently, Pacer^{S157A} and Pacer^{S157D} exhibited differential autophagic activity compared with Pacer^{WT} in GFP-LC3 cleavage (Figure 3C) and p62 degradation assays both *in vitro* (Figure S3C) and *in vivo* (Figures 3D and 3E). Moreover, the inhibitory effect of Pacer S157 phosphorylation on autophagy flux was also revealed by lipid droplet clearance assay (Figures S3D and S3E), autophagosome maturation measurement (Figures 3F and 3G), and transmission electron microscopy analysis (Figures S3F and S3G; Klionsky et al., 2016). These results demonstrate that mTORC1-mediated Pacer phosphorylation at S157 inhibits autophagosome maturation by disrupting the association of Pacer with Stx17 and the HOPS complex.

Pacer S157 Phosphorylation Regulates Pacer Acetylation at Its C-Terminal RH Domain

It was puzzling that the association of Pacer with the HOPS complex was enhanced by S157 de-phosphorylation because Pacer^{100–200aa}, which contains the S157 residue, is not required for HOPS complex association (Cheng et al., 2017). Therefore, we postulated that other post-translational modifications may occur under stressed conditions where mTORC1 is suppressed and Pacer S157 is de-phosphorylated accordingly. Indeed, both endogenous and exogenous Pacers appeared to be acetylated, which was further enhanced by the presence of deacetylase inhibitors (Figures 4A and S4A). Notably, Pacer^{S157A} was hyper-acetylated, whereas Pacer^{S157D} was hypo-acetylated

(Figure 4B), which strongly suggested that Pacer S157 phosphorylation hampered Pacer acetylation. Consistently, mTORC1 inhibition by nutrient deprivation or by Torin1 treatment led to Pacer hyper-acetylation (Figures 4C, 4D, and S4B), which could be reversed by refeeding cells with complete medium (Figures 4C and S4B). These data indicated that mTORC1 indirectly regulated Pacer acetylation through S157 phosphorylation. Importantly, increasing Pacer acetylation levels by addition of deacetylase inhibitors enhanced Pacer-HOPS interaction (Figure 4E), phenocopying Pacer^{S157A}. It has been shown that autophagy activity in mice is maintained at low levels during the embryonic period, whereas it peaks at 3–6 h after birth, particularly in heart tissues (Kuma et al., 2004; Lin et al., 2012). To measure Pacer acetylation and autophagy flux at the organ level, mouse heart homogenates were isolated from neonatal mice or prenatal mouse embryos. We observed that the acetylation levels of Pacer in the mouse heart were significantly increased 24 h after birth and were correlated with decreased Pacer phosphorylation and elevated autophagy flux, which was evidenced by accelerated degradation of p62 (Figures 4F and S4C). To gain further evidence of Pacer acetylation, we purified endogenous Pacer and FLAG-Pacer from starved or Torin1-treated HEK293 cells for mass spectrometry analysis, which resulted in identification of five conserved lysine (K) residues (K483, K523, K533, K573, and K633) as Pacer acetylation sites (Figures 4G and S4D). All of these acetylation sites are located within the Pacer RH domain, which is responsible for binding to the HOPS complex. Individually mutating these lysine residues into arginine (R) slightly diminished Pacer acetylation levels, whereas simultaneous mutation of these five residues totally abolished Pacer acetylation (Figure 4H). Furthermore, the acetylation assay showed that Pacer acetylation levels in the Pacer S157A mutant background were significantly higher than that in the Pacer^{WT} background in both normal and starvation (Earle's balanced salt solution [EBSS]) media (Figures 4I, 4J, and S4E). More importantly, mutating these lysine residues was able to abolish Pacer acetylation. Therefore, Pacer is acetylated *in vitro* and *in vivo* at its RH domain, which is negatively regulated by mTORC1-mediated S157 phosphorylation.

The GSK3-TIP60 Pathway Regulates Pacer Acetylation

Acetylation of autophagy core protein machineries has recently emerged as a crucial mechanism underlying autophagy regulation (Bánréti et al., 2013; Hamaï and Codogno, 2012; Huang et al., 2015; Lee and Finkel, 2009; Lin et al., 2012; McEwan and Dikic, 2011; Su et al., 2017; Xie et al., 2015; Yi et al., 2012). Protein acetylation is catalyzed by lysine acetyltransferases, which are grouped into three major families: GNAT,

(F) The levels of Pacer acetylation in mouse embryos and neonates. Pacer from heart homogenates was isolated from 24 h after birth or prenatal mouse embryos by IP. Autophagy activity was measured by analyzing p62 levels. Acetylation assay methods were as in (D).

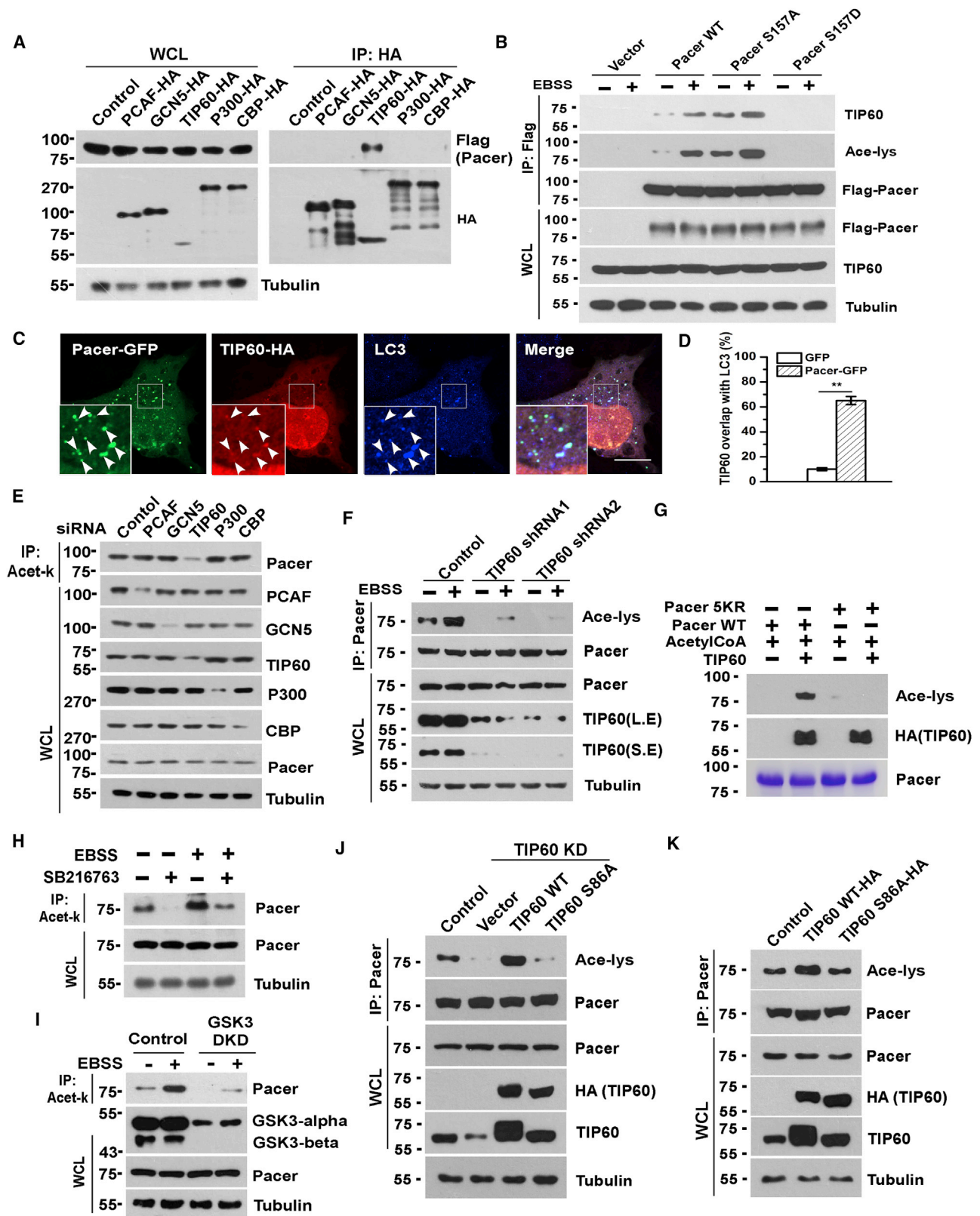
(G) Sequence homology analysis of Pacer acetylation sites. The red K indicates the corresponding conserved lysine.

(H) Acetylation assay of Pacer acetylation site mutants in HEK293T cells. HEK293T cells were transfected with Pacer^{WT}, Pacer^{K483R}, Pacer^{K523R}, Pacer^{K533R}, Pacer^{K573R}, Pacer^{K633R}, or Pacer^{S157A}. Acetylation assay methods were as in (A). 5KR, all five lysine residues were replaced by arginine.

(I) Acetylation assay of Pacer^{2KR} and Pacer^{5KR} in a Pacer^{WT} or Pacer^{S157A} mutant background under normal medium and EBSS medium.

(J) The levels of Pacer acetylation in (I) were quantified by a phosphor-imager and normalized with that of tubulin.

Data are shown as mean ± SD; **p < 0.01, n = 3. See also Figure S4.



(legend on next page)

MYST, and p300/CBP (Allis et al., 2007; Berndsen and Denu, 2008). To identify the acetyltransferase for Pacer acetylation, we collected representative enzymes from these families and conducted a coimmunoprecipitation (coIP) screen. Pacer appeared to selectively interact with TIP60 (Figure 5A). Pacer^{Δ(101–300)}, a mutant containing the C-terminal RH domain, was able to coimmunoprecipitate with TIP60 (Figure 5A). Pacer^{S157A} bound to TIP60 in a more efficient manner than Pacer^{WT}, whereas Pacer^{S157D} exhibited reduced association (Figure 5B), and their interaction was increased by starvation, which was demonstrated by coIP (Figures 5B and S5B) and biochemical fractionation assays (Figure S5C). Indeed, Pacer was able to colocalize with TIP60 on autophagic structures (Figures 5C, 5D, and S5D). Furthermore, small interfering RNA (siRNA) or short hairpin RNA (shRNA)-mediated depletion of TIP60, but not other acetyltransferases, reduced endogenous Pacer acetylation (Figures 5E, 5F, S5E, and S5F). *In vitro* acetylation assays followed by western blot and mass spectrometry analysis further confirmed that TIP60 acetylated Pacer at the five lysine residues (Figures 5G, S5G, and S5H). Previous studies have shown that GSK3 phosphorylates TIP60 at serine 86 (S86) (Charvet et al., 2011; Lin et al., 2012; Nie et al., 2016), which is essential for TIP60 activation. Indeed, suppressing GSK3 signaling with the GSK3 inhibitor SB216763 or by double knockdown (DKD) of GSK3 α and GSK3 β reduced Pacer acetylation (Figures 5H and 5I). Consistently, the loss-of-function mutant TIP60^{S86A}, which was generated by mutating S86 to alanine, failed to rescue the defect of Pacer acetylation in TIP60-depleted HEK293 cells (Figure 5J). Similarly, overexpression of TIP60^{WT} but not TIP60^{S86A} enhanced Pacer acetylation (Figures 5K, S5J, and S5K). Together, these results show that the GSK3-TIP60 signaling pathway directly regulates Pacer acetylation, which is antagonized by mTORC1 through Pacer S157 phosphorylation.

Pacer Acetylation Is Required for Autophagosome Maturation and Cellular Lipid Metabolism

To understand the biological function of Pacer acetylation, we overexpressed Pacer mutants separately and investigated their effect on autophagic flux by measuring p62 levels. We observed that Pacer^{K483R} or Pacer^{K573R} (but not Pacer^{K523R}, Pacer^{K533R}, or Pacer^{K633R}) impaired autophagic flux (Figure 6A), which suggested that K483 and K573 are the key residues targeted by

the GSK3-TIP60 pathway for tuning Pacer function in autophagy. As expected, simultaneously mutating all five lysine residues or K483 and K573 only to arginine (Pacer^{5R} or Pacer^{2R}) significantly ablated Pacer autophagic activity both *in vitro* (Figures 6A, S6A, and S6B) and *in vivo* (Figures 6B and 6C). These observations were further validated by GFP-LC3 cleavage assays (Figure 6D) and mCherry-GFP-LC3 fluorescence microscopy analysis (Figures S6C and S6D). Mechanistically, Pacer^{2R} failed to interact with the HOPS complex and Stx17 as efficiently as Pacer^{WT} under normal culture and starved conditions (Figure 6E). Likewise, TIP60 knockdown reduced Pacer acetylation levels and impaired Pacer association with Stx17 and HOPS at endogenous levels (Figure S6E). These results demonstrated that TIP60-mediated Pacer acetylation facilitates its interaction with the HOPS complex and Stx17, leading to enhanced autophagy flux. Next we conducted lipid droplet clearance assays because autophagy regulates lipid metabolism (Singh et al., 2009), and we observed that Pacer knockdown (KD) resulted in lipid accumulation in a similar manner as observed after Atg5 KD or Atg7 KD, and this defect was rescued by re-expression of Pacer^{WT} but not by Pacer^{2R} (Figure 6F–6H and S6F). In addition, we also confirmed that Pacer dephosphorylation (Pacer S157A) increased autophagic flux, depending on its acetylation (Figures S6G and S6H). Therefore, it is apparent that Pacer acetylation positively regulates autophagosome maturation and cellular lipid metabolism.

Pacer Hypo-acetylation Is Implicated in Nonalcoholic Fatty Liver Disease in Mice

To gain further evidence that Pacer acetylation is involved in autophagy and lipid metabolism *in vivo*, we set up a mouse model of nonalcoholic fatty liver disease (NAFLD) by feeding mice a high-fat diet (HFD) (Figures S7A and S7B). We found that an HFD decreased Pacer acetylation levels in mouse livers, which was accompanied by mTORC1 and AKT activation, GSK3 inactivation, and p62 accumulation (Figure 7A). These observations indicated that an HFD caused impaired liver autophagy and aberrant signaling in lipid metabolism, which was associated with Pacer hypo-acetylation. Next, NAFLD mice were intraperitoneally injected with a recombinant adeno-associated virus (rAAV) expressing either Pacer^{WT} or the permanently deacetylated Pacer mutant (Pacer^{2KR}). The appearance and lipid levels of mouse livers were subsequently examined. Livers

Figure 5. Pacer Was Acetylated by the GSK3-TIP60 Pathway under Nutrient Deprivation

- (A) The interaction of Pacer and acetyltransferase. HA-tagged PCAF, GCN5, TIP60, P300, or CBP was expressed individually in HEK293T stable cells expressing Pacer-FLAG. Anti-HA IP was performed, which was followed by western blot for Pacer-FLAG.
- (B) Analysis of the interaction between Pacer S157 mutants and TIP60.
- (C) Analysis of TIP60, Pacer, and LC3 co-localization. Scale bars, 10 μ m.
- (D) Quantification of the colocalization of TIP60 and LC3. For quantification, cells were counted for each pair of colocalization analyses. Data are shown as mean \pm SD; **p < 0.01, n = 30.
- (E) Acetylation assay of endogenous Pacer in HEK293T cells that were transfected with siRNA targeting PCAF, GCN5, TIP60, P300, or CBP.
- (F) Pacer acetylation assay in control HEK293T cell and shRNA KD TIP60 HEK293T cells under normal medium and EBSS medium for 1 h.
- (G) Pacer acetylation by TIP60 *in vitro*.
- (H) Analysis of endogenous Pacer acetylation upon treatment with EBSS or the GSK3 inhibitor SB216763.
- (I) Analysis of endogenous Pacer acetylation in GSK3 α and GSK3 β DKD HEK293T cells.
- (J) Analysis of endogenous Pacer acetylation in TIP60 KD HEK293T cells, which were rescued with vector, TIP60^{WT} or TIP60^{S86A}.
- (K) Analysis of Pacer acetylation in HEK293T cells expressing TIP60^{WT} or TIP60^{S86A}.

See also Figure S5.

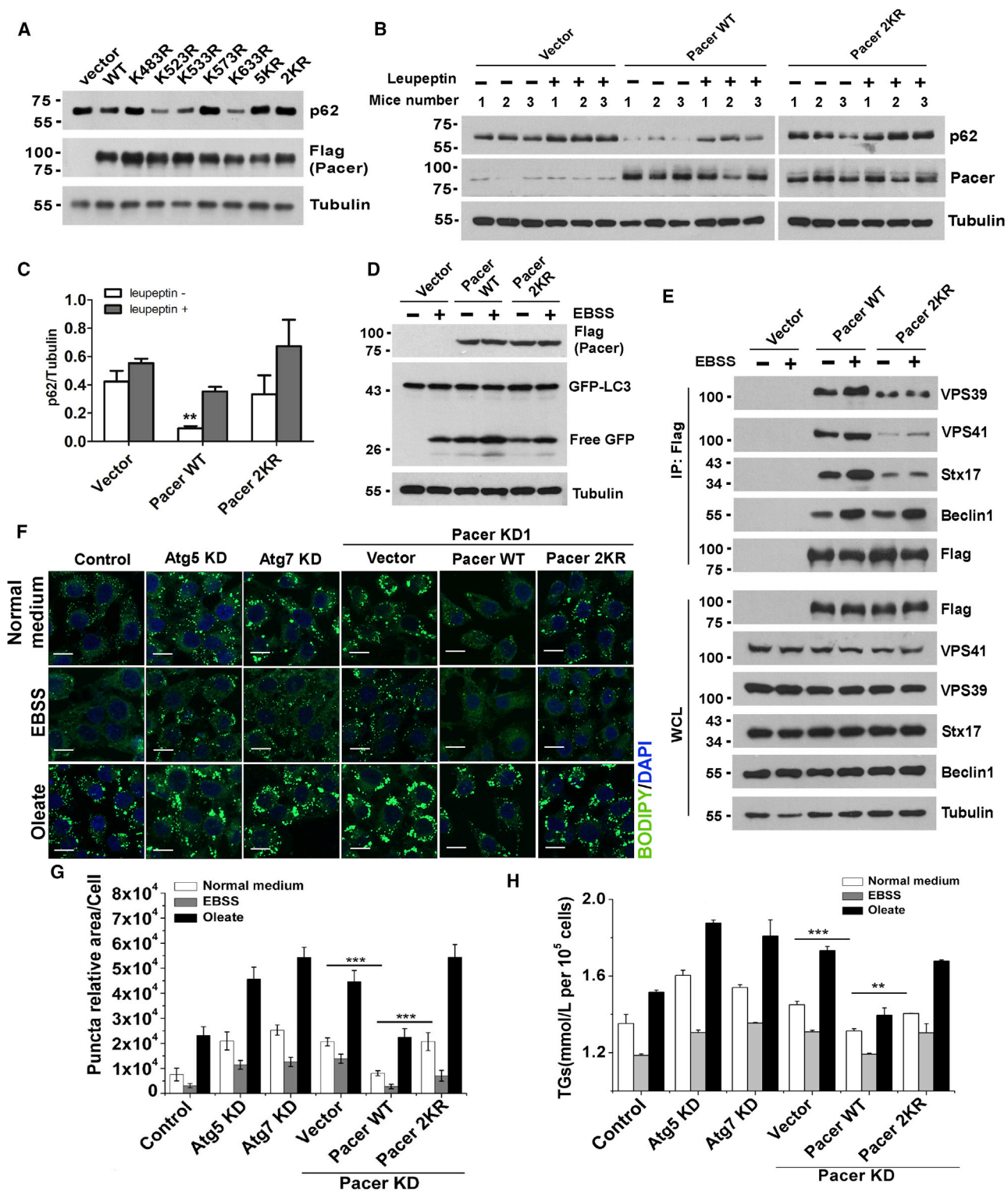


Figure 6. Pacer Acetylation Is Required for Autophagosome Maturation and Lipid Metabolism

(A) Autophagy flux assay in HEK293T cells that were transfected with Pacer K483R, K523R, K533R, K573R, K633R, 5KR, or 2KR and then analyzed by western blot for p62.

(B) Autophagy flux assay in mouse livers. Mice were intraperitoneally injected with HA-tagged rAAV Pacer^{WT} or Pacer^{2KR} and treated with or without 40 mg/kg leupeptin for 12 h. Liver autophagy levels were analyzed by p62 degradation using western blot. n = 3.

(legend continued on next page)

from Pacer^{WT}-injected mice exhibited a red color and dramatically reduced lipid content, similar to the livers from control mice with a normal diet (Figure S7C). In contrast, livers from Pacer^{2KR}-injected mice were pale and filled with lipids, which resembled the livers from control HFD mice. These observations were confirmed by histological oil red O staining and transmission electron microscopy (TEM) analysis (Figures 7B–7F). Consistently, administration of Pacer^{WT}, but not Pacer^{2KR}, was able to restore autophagic flux (Figures S7D–S7F) and alleviate liver damage, as measured by p62 levels and serum alanine aminotransferase or aspartate aminotransferase (ALT or AST) activities, respectively (Figures 7G and 7H). These results demonstrate that Pacer acetylation is required for autophagy flux and lipid metabolism *in vivo*.

DISCUSSION

This study identified a previously unknown signal integration mechanism underlying autophagosome maturation and liver metabolism in response to nutrient deficiency and growth factor deprivation. Our results indicate that Pacer is regulated post-transcriptionally by nutrients and growth factors and serves as a key player in connecting metabolic signals to late steps of autophagy regulation. Importantly, the absence of Pacer impairs autophagosome maturation and lipid catabolism *in vitro* and *in vivo*, whereas Pacer overexpression causes the opposite effects and alleviates HFD-associated metabolic syndrome in mice.

Our results suggest that mTORC1 may extensively participate in the regulation of late stages of autophagy, which involves dynamic assembly and disassembly of autophagy protein machineries at the interface of the lysosome and autophagosome. mTORC1 is activated on the surface of lysosomal membranes (Saxton and Sabatini, 2017). During autolysosome formation, the close proximity of activated lysosomal mTORC1 to autophagosomes enforces the notion that mTORC1, to repress autophagosome maturation, might also target other autophagy protein machineries, including, but not limited to, Rab7 (Jäger et al., 2004; Sun et al., 2010; Tabata et al., 2010), HDAC6 (Lee et al., 2010), the HOPS complex (Ho and Stroupe, 2015; Jiang et al., 2014; Liang et al., 2008; Takáts et al., 2014; Wartosch et al., 2015), Stx17 (Itakura et al., 2012), TECPR1 (Chen et al., 2012), PLEKHM1 (McEwan et al., 2015; Tabata et al., 2010), Atg14(L) (Diao et al., 2015), and EPG5 (Wang et al., 2016).

This work, together with studies by others, demonstrates that the GSK3-TIP60 signaling axis is involved in both early and late stages of autophagy regulation (Lin et al., 2012; Yi et al., 2012). However, it remains elusive how these func-

tions are temporally and spatially coordinated (Hamaï and Codogno, 2012). Presumably, under stressed conditions, GSK3-mediated TIP60 phosphorylation and activation facilitate its sequential interaction with ULK1 on isolation membranes, Atg3 on elongating membranes, and Pacer on autophagosomes, which results in acetylation-mediated autophagy stimulation at different stages. Indeed, nutrient deprivation enhances the association of TIP60 with ULK1 (Lin et al., 2012) or Pacer (Figures 5B and S4A) through phosphorylation. In addition, TIP60 Ser86 phosphorylation, ULK1 acetylation (Lin et al., 2012), and Pacer acetylation (Figure 4E) correlated with the enhanced autophagic flux that occurs in the first few days after mouse birth. Consistently, crucial roles of TIP60 in the autophagy pathway were also implied by mouse genetic studies *in vivo* (Hamaï and Codogno, 2012; Hu et al., 2009; Mizushima and Komatsu, 2011).

Autophagy plays essential roles in liver metabolic homeostasis (Kaur and Debnath, 2015; Madrigal-Matute and Cuervo, 2016; Schneider and Cuervo, 2014). Our data from the liver-specific Pacer knockout mouse model indicate that Pacer regulates liver homeostasis as an important autophagy enhancer (Figure 1). In addition, our previous study showed that Rubicon antagonizes Pacer in autophagy modulation. In line with these observations, liver-specific knockout of Rubicon increased hepatic autophagy flux and alleviated HFD-induced liver steatosis (Tanaka et al., 2016). Therefore, Pacer and Rubicon appear to form a molecular switch both *in vitro* and *in vivo* for adjustment of autophagy activity and for maintenance of tissue homeostasis. Notably, studies have shown that an aging-dependent reduction in autophagic activity is frequently implicated in the pathogenesis of liver diseases (Ueno and Komatsu, 2017). Indeed, Pacer hypoacetylation, which is indicative of low autophagy activity, occurs during the pathogenesis of NAFLD in mice (Figure 7A). Enforced overexpression of Pacer^{WT}, but not the autophagy-defective mutant Pacer^{2KR}, was able to alleviate NAFLD symptoms in mice (Figures 7 and S6). This appears to be functionally equivalent to pharmacologically enhancing autophagy using rapamycin (Lin et al., 2013), which increases Pacer acetylation and autophagic activity by inhibiting mTORC1 (Figure 4D).

The signaling axis uncovered in this study may also exist and function in other tissues or organs besides the liver because Pacer appears to be ubiquitously expressed (unpublished data). Autophagy modulation has been intensely investigated in the laboratory and the clinic for drug development (Rubinsztein et al., 2012), and essential autophagy upstream regulators such as mTORC1 and GSK3 are major drug targets for treatment of various human diseases (Beurel et al., 2015; Cohen and Goedert, 2004). Therefore, the identification of Pacer as a mediator of

(C) Statistical analysis of p62 in (B). Data are shown as mean \pm SD; **p < 0.01, n = 3.

(D) GFP-LC3 cleavage assay. HEK293T stable cell lines harboring the GFP-LC3 vector were transfected with vector, FLAG-tagged Pacer^{WT}, or Pacer^{2KR}, and the free GFP fragment was detected by western blot using an anti-GFP antibody.

(E) The interaction of Pacer^{2KR} and Stx17-HOPS subunits. FLAG-tagged Pacer^{WT} or Pacer^{2KR} was expressed individually in HEK293T cells that were treated without/with EBSS for 1 h. IP was performed with anti-FLAG beads, and samples were immunoblotted for endogenous Stx17, VPS39, and VPS41.

(F) Lipid droplet (LD) clearance assay in Atg5 KD, Atg7 KD, Pacer KD that was rescued by vector, Pacer^{WT}, or Pacer^{2KR}. LO2 cells were cultured with normal medium, normal medium plus oleate (OL) for 4 h, or EBSS for 1 h. Green, BODIPY lipid probes 493/503; blue, DAPI. Scale bar, 10 μ m.

(G) Quantification of LDs in (F). Data are shown as mean \pm SD from 30 micrographs of three independent experiments; ***p < 0.001, n = 30.

(H) Triglyceride (TG) levels in LO2 cells as indicated. Data are shown as mean \pm SD; ***p < 0.001, n = 3.

See also Figure S6.

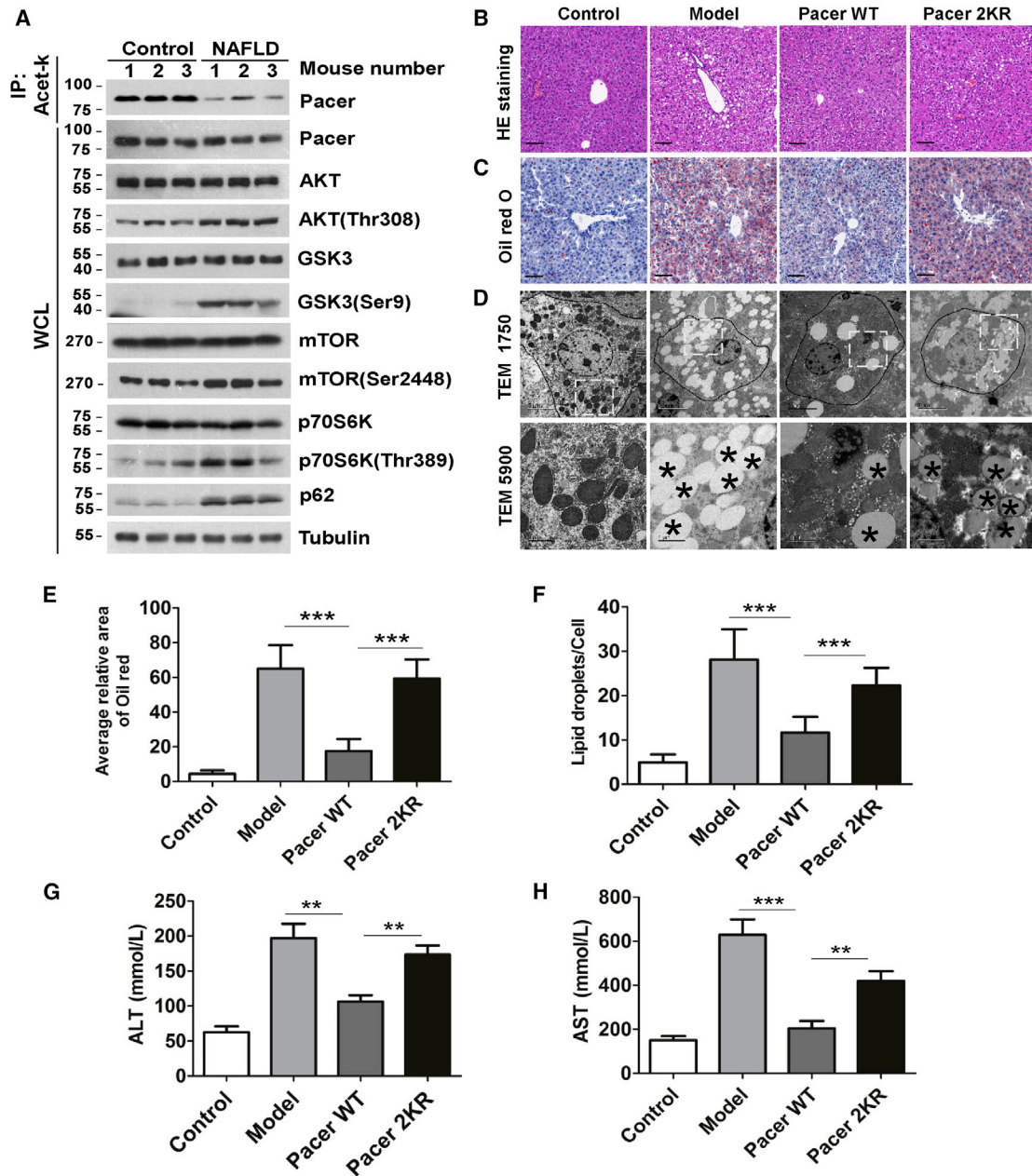


Figure 7. Pacer Hypo-acetylation Is Implicated in NAFLD in Mice

(A) Hepatic expression levels of acet-Pacer and proteins, as indicated, by western blot.

(B) H&E staining showing liver histopathologic changes in NAFLD mice of the control group, model group, AAV-Pacer^{WT} group, and AAV-Pacer^{2KR} group. Scale bars, 100 μ m; 200 \times , n = 7.

(C) Oil red O staining of liver sections in NAFLD mice of the control group, model group, AAV-Pacer^{WT} group, and AAV-Pacer^{2KR} group. Scale bars, 100 μ m; 200 \times , n = 7.

(D) LDs by transmission electron microscopy in NAFLD mice of the control group, model group, AAV-Pacer^{WT} group, and AAV-Pacer^{2KR} group. n = 7.

(E) Quantification of oil red O staining in (C). Data are shown as mean \pm SD from 30 micrographs of three independent experiments; ***p < 0.001.

(F) Quantification of LDs in (D). Data are shown as mean \pm SD from 30 micrographs of three independent experiments; ***p < 0.001.

(G) ALT assays in NAFLD mice of the control group, model group, AAV-Pacer^{WT} group, and AAV-Pacer^{2KR} group. Data are shown as mean \pm SD for three independent experiments; **p < 0.01, n = 7.

(H) AST assays in NAFLD mice of the control group, model group, AAV-Pacer^{WT} group, and AAV-Pacer^{2KR} group. Data are shown as mean \pm SD for three independent experiments; **p < 0.01, ***p < 0.001, n = 7.

See also [Figure S7](#).

convergent signaling of mTOR and GSK3 may have major therapeutic implications.

STAR★METHODS

Detailed methods are provided in the online version of this paper and include the following:

- **KEY RESOURCES TABLE**
- **CONTACT FOR REAGENT AND RESOURCE SHARING**
- **EXPERIMENTAL MODEL AND SUBJECT DETAILS**
 - Cell culture
 - Pacer knockout mouse models
 - Non-alcoholic fatty liver disease mouse model
 - Mouse Models of Pacer or mutant overexpression and treatment
- **METHOD DETAILS**
 - p62 degradation assay
 - Autophagosome maturation assay
 - Immunoprecipitation and western blot
 - Immunofluorescence
 - Transmission electron microscopy
 - *In vitro* acetylation assay
 - *In vitro* kinase assay
 - Triglyceride content in liver and cultured hepatocytes
 - Ketone body assay in serum and liver tissues
 - Protein extraction from tissue
 - Fractionation by differential centrifugation
 - RNA Isolation and qPCR Analyses
 - Oil red O staining
 - Hematoxylin and Eosin Staining and Immunohistochemistry
 - *In situ* hybridization
- **QUANTIFICATION AND STATISTICAL ANALYSIS**

SUPPLEMENTAL INFORMATION

Supplemental Information includes seven figures and can be found with this article online at <https://doi.org/10.1016/j.molcel.2018.12.017>.

ACKNOWLEDGMENTS

We thank Prof. Li Yu from Tsinghua University for advice and Prof. Jiahui Han and Prof. Shengcai Lin from Xiamen University for cDNA. We thank the Imaging Center of Zhejiang University School of Medicine for assistance with confocal microscopy and electron microscopy. This study was supported by the Ministry of Science and Technology of the People's Republic of China under grant 2017YFA0503402 (to Q.S.), the National Natural Science Foundation under grants 31771525 and 91754113 (to Q.S.) and 31601119 (to X.C.), and Zhejiang Provincial Funds for Distinguished Young Scientists under grant LR15C070001 (to Q.S.).

AUTHOR CONTRIBUTIONS

Q.S. and X.C. designed the experiments. X.C., Q.Z., X.M., D.S., X.D., R.T., X.J., and H.S. performed the experiments. W.L., Z.S., W.G., and T.L. contributed reagents. L.L. and S.C. performed mass spectrometry. Q.S. and X.C. wrote the manuscript. All authors discussed the results and commented on the manuscript.

DECLARATION OF INTERESTS

The authors declare no competing interests.

Received: March 1, 2018

Revised: July 18, 2018

Accepted: December 19, 2018

Published: January 28, 2019

REFERENCES

- Allis, C.D., Berger, S.L., Cote, J., Dent, S., Jenuwien, T., Kouzarides, T., Pillus, L., Reinberg, D., Shi, Y., Shiekhhattar, R., et al. (2007). New nomenclature for chromatin-modifying enzymes. *Cell* 131, 633–636.
- Bánrétí, A., Sass, M., and Graba, Y. (2013). The emerging role of acetylation in the regulation of autophagy. *Autophagy* 9, 819–829.
- Ben-Sahra, I., and Manning, B.D. (2017). mTORC1 signaling and the metabolic control of cell growth. *Curr. Opin. Cell Biol.* 45, 72–82.
- Berndsen, C.E., and Denu, J.M. (2008). Catalysis and substrate selection by histone/protein lysine acetyltransferases. *Curr. Opin. Struct. Biol.* 18, 682–689.
- Beurel, E., Grieco, S.F., and Jope, R.S. (2015). Glycogen synthase kinase-3 (GSK3): regulation, actions, and diseases. *Pharmacol. Ther.* 148, 114–131.
- Buller, C.L., Loberg, R.D., Fan, M.H., Zhu, Q., Park, J.L., Vesely, E., Inoki, K., Guan, K.L., and Brosius, F.C., 3rd (2008). A GSK-3/TSC2/mTOR pathway regulates glucose uptake and GLUT1 glucose transporter expression. *Am. J. Physiol. Cell Physiol.* 295, C836–C843.
- Chang, Y.Y., and Neufeld, T.P. (2009). An Atg1/Atg13 complex with multiple roles in TOR-mediated autophagy regulation. *Mol. Biol. Cell* 20, 2004–2014.
- Charvet, C., Wissler, M., Brauns-Schubert, P., Wang, S.J., Tang, Y., Sigloch, F.C., Mellert, H., Brandenburg, M., Lindner, S.E., Breit, B., et al. (2011). Phosphorylation of Tip60 by GSK-3 determines the induction of PUMA and apoptosis by p53. *Mol. Cell* 42, 584–596.
- Chen, D., Fan, W., Lu, Y., Ding, X., Chen, S., and Zhong, Q. (2012). A mammalian autophagosome maturation mechanism mediated by TECPR1 and the Atg12-Atg5 conjugate. *Mol. Cell* 45, 629–641.
- Cheng, X., Ma, X., Ding, X., Li, L., Jiang, X., Shen, Z., Chen, S., Liu, W., Gong, W., and Sun, Q. (2017). Pacer Mediates the Function of Class III PI3K and HOPS Complexes in Autophagosome Maturation by Engaging Stx17. *Mol. Cell* 65, 1029–1043.e5.
- Cohen, P., and Goedert, M. (2004). GSK3 inhibitors: development and therapeutic potential. *Nat. Rev. Drug Discov.* 3, 479–487.
- Diao, J., Liu, R., Rong, Y., Zhao, M., Zhang, J., Lai, Y., Zhou, Q., Wilz, L.M., Li, J., Vivona, S., et al. (2015). ATG14 promotes membrane tethering and fusion of autophagosomes to endolysosomes. *Nature* 520, 563–566.
- Egan, D.F., Shackelford, D.B., Mihaylova, M.M., Gelino, S., Kohnz, R.A., Mair, W., Vasquez, D.S., Joshi, A., Gwinn, D.M., Taylor, R., et al. (2011). Phosphorylation of ULK1 (hATG1) by AMP-activated protein kinase connects energy sensing to mitophagy. *Science* 331, 456–461.
- Ganley, I.G., Lam, H., Wang, J., Ding, X., Chen, S., and Jiang, X. (2009). ULK1.ATG13.FIP200 complex mediates mTOR signaling and is essential for autophagy. *J. Biol. Chem.* 284, 12297–12305.
- Guo, B., Liang, Q., Li, L., Hu, Z., Wu, F., Zhang, P., Ma, Y., Zhao, B., Kovács, A.L., Zhang, Z., et al. (2014). O-GlcNAc-modification of SNAP-29 regulates autophagosome maturation. *Nat. Cell Biol.* 16, 1215–1226.
- Hamaï, A., and Codogno, P. (2012). New targets for acetylation in autophagy. *Sci. Signal.* 5, pe29.
- He, C., and Klionsky, D.J. (2009). Regulation mechanisms and signaling pathways of autophagy. *Annu. Rev. Genet.* 43, 67–93.
- Ho, R., and Stroupe, C. (2015). The HOPS/class C Vps complex tethers membranes by binding to one Rab GTPase in each apposed membrane. *Mol. Biol. Cell* 26, 2655–2663.
- Hosokawa, N., Hara, T., Kaizuka, T., Kishi, C., Takamura, A., Miura, Y., Iemura, S., Natsume, T., Takehana, K., Yamada, N., et al. (2009). Nutrient-dependent mTORC1 association with the ULK1-Atg13-FIP200 complex required for autophagy. *Mol. Biol. Cell* 20, 1981–1991.
- Hsu, P.P., Kang, S.A., Rameseder, J., Zhang, Y., Ottina, K.A., Lim, D., Peterson, T.R., Choi, Y., Gray, N.S., Yaffe, M.B., et al. (2011). The

- mTOR-regulated phosphoproteome reveals a mechanism of mTORC1-mediated inhibition of growth factor signaling. *Science* 332, 1317–1322.
- Hu, Y., Fisher, J.B., Koprowski, S., McAllister, D., Kim, M.S., and Lough, J. (2009). Homozygous disruption of the Tip60 gene causes early embryonic lethality. *Dev. Dyn.* 238, 2912–2921.
- Huang, R., Xu, Y., Wan, W., Shou, X., Qian, J., You, Z., Liu, B., Chang, C., Zhou, T., Lippincott-Schwartz, J., and Liu, W. (2015). Deacetylation of nuclear LC3 drives autophagy initiation under starvation. *Mol. Cell* 57, 456–466.
- Itakura, E., Kishi-Itakura, C., and Mizushima, N. (2012). The hairpin-type tail-anchored SNARE syntaxin 17 targets to autophagosomes for fusion with endosomes/lysosomes. *Cell* 151, 1256–1269.
- Jäger, S., Bucci, C., Tanida, I., Ueno, T., Kominami, E., Saftig, P., and Eskelinen, E.L. (2004). Role for Rab7 in maturation of late autophagic vacuoles. *J. Cell Sci.* 117, 4837–4848.
- Jiang, P., Nishimura, T., Sakamaki, Y., Itakura, E., Hatta, T., Natsume, T., and Mizushima, N. (2014). The HOPS complex mediates autophagosome-lysosome fusion through interaction with syntaxin 17. *Mol. Biol. Cell* 25, 1327–1337.
- Jung, C.H., Jun, C.B., Ro, S.H., Kim, Y.M., Otto, N.M., Cao, J., Kundu, M., and Kim, D.H. (2009). ULK-Atg13-FIP200 complexes mediate mTOR signaling to the autophagy machinery. *Mol. Biol. Cell* 20, 1992–2003.
- Karsli-Uzunbas, G., Guo, J.Y., Price, S., Teng, X., Laddha, S.V., Khor, S., Kalaany, N.Y., Jacks, T., Chan, C.S., Rabinowitz, J.D., and White, E. (2014). Autophagy is required for glucose homeostasis and lung tumor maintenance. *Cancer Discov.* 4, 914–927.
- Kaur, J., and Debnath, J. (2015). Autophagy at the crossroads of catabolism and anabolism. *Nat. Rev. Mol. Cell Biol.* 16, 461–472.
- Kim, J., Kundu, M., Viollet, B., and Guan, K.L. (2011). AMPK and mTOR regulate autophagy through direct phosphorylation of Ulk1. *Nat. Cell Biol.* 13, 132–141.
- Kim, Y.M., Jung, C.H., Seo, M., Kim, E.K., Park, J.M., Bae, S.S., and Kim, D.H. (2015). mTORC1 phosphorylates UVRAG to negatively regulate autophagosome and endosome maturation. *Mol. Cell* 57, 207–218.
- Klionsky, D.J., Abdelmohsen, K., Abe, A., Abedin, M.J., Abeliovich, H., Acevedo Arozena, A., Adachi, H., Adams, C.M., Adams, P.D., Adeli, K., et al. (2016). Guidelines for the use and interpretation of assays for monitoring autophagy (3rd edition). *Autophagy* 12, 1–222.
- Komatsu, M., Waguri, S., Ueno, T., Iwata, J., Murata, S., Tanida, I., Ezaki, J., Mizushima, N., Ohsumi, Y., Uchiyama, Y., et al. (2005). Impairment of starvation-induced and constitutive autophagy in Atg7-deficient mice. *J. Cell Biol.* 169, 425–434.
- Komatsu, M., Waguri, S., Koike, M., Sou, Y.S., Ueno, T., Hara, T., Mizushima, N., Iwata, J., Ezaki, J., Murata, S., et al. (2007). Homeostatic levels of p62 control cytoplasmic inclusion body formation in autophagy-deficient mice. *Cell* 131, 1149–1163.
- Kroemer, G., Mariño, G., and Levine, B. (2010). Autophagy and the integrated stress response. *Mol. Cell* 40, 280–293.
- Ktistakis, N.T., and Tooze, S.A. (2016). Digesting the Expanding Mechanisms of Autophagy. *Trends Cell Biol.* 26, 624–635.
- Kuma, A., Hatano, M., Matsui, M., Yamamoto, A., Nakaya, H., Yoshimori, T., Ohsumi, Y., Tokuhisa, T., and Mizushima, N. (2004). The role of autophagy during the early neonatal starvation period. *Nature* 432, 1032–1036.
- Lee, I.H., and Finkel, T. (2009). Regulation of autophagy by the p300 acetyltransferase. *J. Biol. Chem.* 284, 6322–6328.
- Lee, J.Y., Koga, H., Kawaguchi, Y., Tang, W., Wong, E., Gao, Y.S., Pandey, U.B., Kaushik, S., Tresse, E., Lu, J., et al. (2010). HDAC6 controls autophagosome maturation essential for ubiquitin-selective quality-control autophagy. *EMBO J.* 29, 969–980.
- Liang, C., Lee, J.S., Inn, K.S., Gack, M.U., Li, Q., Roberts, E.A., Vergne, I., Deretic, V., Feng, P., Akazawa, C., and Jung, J.U. (2008). Beclin1-binding UVRAG targets the class C Vps complex to coordinate autophagosome maturation and endocytic trafficking. *Nat. Cell Biol.* 10, 776–787.
- Lin, S.Y., Li, T.Y., Liu, Q., Zhang, C., Li, X., Chen, Y., Zhang, S.M., Lian, G., Liu, Q., Ruan, K., et al. (2012). GSK3-TIP60-ULK1 signaling pathway links growth factor deprivation to autophagy. *Science* 336, 477–481.
- Lin, C.W., Zhang, H., Li, M., Xiong, X., Chen, X., Chen, X., Dong, X.C., and Yin, X.M. (2013). Pharmacological promotion of autophagy alleviates steatosis and injury in alcoholic and non-alcoholic fatty liver conditions in mice. *J. Hepatol.* 58, 993–999.
- Ma, X., Zhang, S., He, L., Rong, Y., Brier, L.W., Sun, Q., Liu, R., Fan, W., Chen, S., Yue, Z., et al. (2017). MTORC1-mediated NRFB2 phosphorylation functions as a switch for the class III PtdIns3K and autophagy. *Autophagy* 13, 592–607.
- Mack, H.I., Zheng, B., Asara, J.M., and Thomas, S.M. (2012). AMPK-dependent phosphorylation of ULK1 regulates ATG9 localization. *Autophagy* 8, 1197–1214.
- Madrigal-Matute, J., and Cuervo, A.M. (2016). Regulation of Liver Metabolism by Autophagy. *Gastroenterology* 150, 328–339.
- Martina, J.A., Chen, Y., Gucek, M., and Puertollano, R. (2012). MTORC1 functions as a transcriptional regulator of autophagy by preventing nuclear transport of TFEB. *Autophagy* 8, 903–914.
- Martinez-Lopez, N., and Singh, R. (2015). Autophagy and Lipid Droplets in the Liver. *Annu. Rev. Nutr.* 35, 215–237.
- McEwan, D.G., and Dikic, I. (2011). The Three Musketeers of Autophagy: phosphorylation, ubiquitylation and acetylation. *Trends Cell Biol.* 21, 195–201.
- McEwan, D.G., Popovic, D., Gubas, A., Terawaki, S., Suzuki, H., Stadel, D., Coxon, F.P., Miranda de Stegmann, D., Bhogaraju, S., Maddi, K., et al. (2015). PLEKHM1 regulates autophagosome-lysosome fusion through HOPS complex and LC3/GABARAP proteins. *Mol. Cell* 57, 39–54.
- Mizushima, N., and Komatsu, M. (2011). Autophagy: renovation of cells and tissues. *Cell* 147, 728–741.
- Mizushima, N., Levine, B., Cuervo, A.M., and Klionsky, D.J. (2008). Autophagy fights disease through cellular self-digestion. *Nature* 451, 1069–1075.
- Mizushima, N., Yoshimori, T., and Ohsumi, Y. (2011). The role of Atg proteins in autophagosome formation. *Annu. Rev. Cell Dev. Biol.* 27, 107–132.
- Munson, M.J., Allen, G.F., Toth, R., Campbell, D.G., Lucocq, J.M., and Ganley, I.G. (2015). mTOR activates the VPS34-UVRAG complex to regulate autolysosomal tubulation and cell survival. *EMBO J.* 34, 2272–2290.
- Nazio, F., Strappazzon, F., Antonioni, M., Bielli, P., Cianfanelli, V., Bordi, M., Gretzmeier, C., Dengjel, J., Piacentini, M., Fimia, G.M., and Cecconi, F. (2013). mTOR inhibits autophagy by controlling ULK1 ubiquitylation, self-association and function through AMBRA1 and TRAF6. *Nat. Cell Biol.* 15, 406–416.
- Nie, T., Yang, S., Ma, H., Zhang, L., Lu, F., Tao, K., Wang, R., Yang, R., Huang, L., Mao, Z., and Yang, Q. (2016). Regulation of ER stress-induced autophagy by GSK3 β -TIP60-ULK1 pathway. *Cell Death Dis.* 7, e2563.
- Roczniak-Ferguson, A., Petit, C.S., Froehlich, F., Qian, S., Ky, J., Angarola, B., Walther, T.C., and Ferguson, S.M. (2012). The transcription factor TFEB links mTORC1 signaling to transcriptional control of lysosome homeostasis. *Sci. Signal.* 5, ra42.
- Rubinsztein, D.C., Codogno, P., and Levine, B. (2012). Autophagy modulation as a potential therapeutic target for diverse diseases. *Nat. Rev. Drug Discov.* 11, 709–730.
- Saxton, R.A., and Sabatini, D.M. (2017). mTOR Signaling in Growth, Metabolism, and Disease. *Cell* 168, 960–976.
- Schneider, J.L., and Cuervo, A.M. (2014). Liver autophagy: much more than just taking out the trash. *Nat. Rev. Gastroenterol. Hepatol.* 11, 187–200.
- Settembre, C., Zoncu, R., Medina, D.L., Vetrini, F., Erdin, S., Erdin, S., Huynh, T., Ferron, M., Karsenty, G., Vellard, M.C., et al. (2012). A lysosome-to-nucleus signalling mechanism senses and regulates the lysosome via mTOR and TFEB. *EMBO J.* 31, 1095–1108.
- Shang, L., and Wang, X. (2011). AMPK and mTOR coordinate the regulation of ULK1 and mammalian autophagy initiation. *Autophagy* 7, 924–926.
- Shin, S., Wolgamott, L., Yu, Y., Blenis, J., and Yoon, S.O. (2011). Glycogen synthase kinase (GSK)-3 promotes p70 ribosomal protein S6 kinase

- (p70S6K) activity and cell proliferation. *Proc. Natl. Acad. Sci. USA* *108*, E1204–E1213.
- Singh, R., Kaushik, S., Wang, Y., Xiang, Y., Novak, I., Komatsu, M., Tanaka, K., Cuervo, A.M., and Czaja, M.J. (2009). Autophagy regulates lipid metabolism. *Nature* *458*, 1131–1135.
- Su, H., Yang, F., Wang, Q., Shen, Q., Huang, J., Peng, C., Zhang, Y., Wan, W., Wong, C.C.L., Sun, Q., et al. (2017). VPS34 Acetylation Controls Its Lipid Kinase Activity and the Initiation of Canonical and Non-canonical Autophagy. *Mol. Cell* *67*, 907–921.e7.
- Sun, Q., Westphal, W., Wong, K.N., Tan, I., and Zhong, Q. (2010). Rubicon controls endosome maturation as a Rab7 effector. *Proc. Natl. Acad. Sci. USA* *107*, 19338–19343.
- Sun, T., Li, X., Zhang, P., Chen, W.D., Zhang, H.L., Li, D.D., Deng, R., Qian, X.J., Jiao, L., Ji, J., et al. (2015). Acetylation of Beclin 1 inhibits autophagosome maturation and promotes tumour growth. *Nat. Commun.* *6*, 7215.
- Tabata, K., Matsunaga, K., Sakane, A., Sasaki, T., Noda, T., and Yoshimori, T. (2010). Rubicon and PLEKHM1 negatively regulate the endocytic/autophagic pathway via a novel Rab7-binding domain. *Mol. Biol. Cell* *21*, 4162–4172.
- Takamura, A., Komatsu, M., Hara, T., Sakamoto, A., Kishi, C., Waguri, S., Eishi, Y., Hino, O., Tanaka, K., and Mizushima, N. (2011). Autophagy-deficient mice develop multiple liver tumors. *Genes Dev.* *25*, 795–800.
- Takáts, S., Piracs, K., Nagy, P., Varga, Á., Kárpáti, M., Hegedűs, K., Kramer, H., Kovács, A.L., Sass, M., and Juhász, G. (2014). Interaction of the HOPS complex with Syntaxin 17 mediates autophagosome clearance in *Drosophila*. *Mol. Biol. Cell* *25*, 1338–1354.
- Tanaka, S., Hikita, H., Tatsumi, T., Sakamori, R., Nozaki, Y., Sakane, S., Shiode, Y., Nakabori, T., Saito, Y., Hiramatsu, N., et al. (2016). Rubicon inhibits autophagy and accelerates hepatocyte apoptosis and lipid accumulation in nonalcoholic fatty liver disease in mice. *Hepatology* *64*, 1994–2014.
- Toshima, T., Shirabe, K., Fukuhara, T., Ikegami, T., Yoshizumi, T., Soejima, Y., Ikeda, T., Okano, S., and Maehara, Y. (2014). Suppression of autophagy during liver regeneration impairs energy charge and hepatocyte senescence in mice. *Hepatology* *60*, 290–300.
- Ueno, T., and Komatsu, M. (2017). Autophagy in the liver: functions in health and disease. *Nat. Rev. Gastroenterol. Hepatol.* *14*, 170–184.
- Wan, W., You, Z., Zhou, L., Xu, Y., Peng, C., Zhou, T., Yi, C., Shi, Y., and Liu, W. (2018). mTORC1-Regulated and HUWE1-Mediated WIPI2 Degradation Controls Autophagy Flux. *Mol. Cell* *72*, 303–315.e6.
- Wang, Z., Miao, G., Xue, X., Guo, X., Yuan, C., Wang, Z., Zhang, G., Chen, Y., Feng, D., Hu, J., and Zhang, H. (2016). The Vici Syndrome Protein EPG5 Is a Rab7 Effector that Determines the Fusion Specificity of Autophagosomes with Late Endosomes/Lysosomes. *Mol. Cell* *63*, 781–795.
- Wartosch, L., Günesdogan, U., Graham, S.C., and Luzio, J.P. (2015). Recruitment of VPS33A to HOPS by VPS16 Is Required for Lysosome Fusion with Endosomes and Autophagosomes. *Traffic* *16*, 727–742.
- Xie, Y., Kang, R., Sun, X., Zhong, M., Huang, J., Klionsky, D.J., and Tang, D. (2015). Posttranslational modification of autophagy-related proteins in macroautophagy. *Autophagy* *11*, 28–45.
- Yi, C., Ma, M., Ran, L., Zheng, J., Tong, J., Zhu, J., Ma, C., Sun, Y., Zhang, S., Feng, W., et al. (2012). Function and molecular mechanism of acetylation in autophagy regulation. *Science* *336*, 474–477.
- Yu, L., McPhee, C.K., Zheng, L., Mardones, G.A., Rong, Y., Peng, J., Mi, N., Zhao, Y., Liu, Z., Wan, F., et al. (2010). Termination of autophagy and reformation of lysosomes regulated by mTOR. *Nature* *465*, 942–946.
- Yu, Y., Yoon, S.O., Poulogiannis, G., Yang, Q., Ma, X.M., Villén, J., Kubica, N., Hoffman, G.R., Cantley, L.C., Gygi, S.P., and Blenis, J. (2011). Phosphoproteomic analysis identifies Grb10 as an mTORC1 substrate that negatively regulates insulin signaling. *Science* *332*, 1322–1326.
- Yuan, H.X., Russell, R.C., and Guan, K.L. (2013). Regulation of PIK3C3/VPS34 complexes by MTOR in nutrient stress-induced autophagy. *Autophagy* *9*, 1983–1995.

Q3 Q4 Q5 STAR★METHODS

KEY RESOURCES TABLE

REAGENT or RESOURCE	SOURCE	IDENTIFIER
Antibodies		
Rabbit polyclonal anti-human Pacer	Homemade	Huabio Hangzhou
Rabbit polyclonal anti-mouse Pacer	Homemade	Huabio Hangzhou
Rabbit polyclonal anti-Pacer(Ser157)	Homemade	Huabio Hangzhou
Rabbit polyclonal anti-Acetylated-Lysine (WB)	Cell Signaling Technology	Cat#9441; AB_331805
Rabbit polyclonal anti-Lamp1	Cell Signaling Technology	Cat#D2D11; RRID:AB_2687579
Rabbit polyclonal anti-UVRAG	Cell Signaling Technology	Cat#D2Q1Z; RRID:AB_2687988
Rabbit monoclonal anti-PCAF	Cell Signaling Technology	Cat#3378; RRID:AB_2128409
Rabbit polyclonal anti-AKT	Cell Signaling Technology	Cat#9272; RRID:AB_329827
Rabbit polyclonal anti-AKT (Thr308)	Cell Signaling Technology	Cat#13038; RRID:AB_2629447
Rabbit polyclonal anti-AKT (Ser473)	Cell Signaling Technology	Cat#4060; RRID:AB_2315049
Rabbit polyclonal anti- GSK-3 α / β	Cell Signaling Technology	Cat#5676; RRID:AB_10547140
Rabbit polyclonal anti- GSK-3 β (Ser9)	Cell Signaling Technology	Cat#5558; RRID:AB_10013750
Rabbit polyclonal anti-mTOR	Cell Signaling Technology	Cat#2983; RRID:AB_2105622
Rabbit polyclonal anti-mTOR(Ser2448)	Cell Signaling Technology	Cat#5536; RRID:AB_10691552
Rabbit polyclonal anti-P70S6K	Cell Signaling Technology	Cat#9202; RRID:AB_331676
Rabbit polyclonal anti-P70S6K(Thr389)	Cell Signaling Technology	Cat#9234; RRID:AB_2269803
Rabbit polyclonal anti-Raptor	Cell Signaling Technology	Cat#2280; RRID:AB_10694695
Rabbit polyclonal anti-Rictor	Cell Signaling Technology	Cat#2114; RRID:AB_10694641
Mouse monoclonal anti-Vps41	Santa Cruz Biotechnology	Cat#sc-377118; RRID:AB_2687987
Mouse monoclonal anti-Vps39	Santa Cruz Biotechnology	Cat#sc-514762; RRID:AB_2687985
Mouse monoclonal anti- Acetylated-lysine (IP)	Santa Cruz Biotechnology	Cat#sc-32268; RRID:AB_627898
Mouse monoclonal anti-GCN5	Santa Cruz Biotechnology	Cat#sc-365321; RRID:AB_10846182
Mouse monoclonal anti-P300	Santa Cruz Biotechnology	Cat#sc-48343; RRID:AB_628075
Mouse monoclonal anti-CBP	Santa Cruz Biotechnology	Cat#sc-7300; RRID:AB_626817
Rabbit polyclonal anti-LC3 (IF)	MBL	Cat#PM036; RRID:AB_2274121
Rabbit polyclonal anti-p62/SQSTM1	MBL	Cat#PM045; RRID:AB_1279301
Rabbit polyclonal anti-Synyaxin-17	MBL	Cat# PM076;
Mouse monoclonal anti-GFP	MBL	Cat#M048-3; RRID:AB_591823
Rabbit polyclonal anti-Beclin1	MBL	Cat#PD017;RRID:AB_1278767
Mouse monoclonal anti-HA-Tag-HRP	MBL	Cat#M180-7; RRID:AB_11124961
Mouse monoclonal anti-Flag-Tag-HRP	MBL	Cat#M185-7; RRID:AB_2687989
Rabbit polyclonal anti-LC3 (WB)	Sigma	Cat#L8918; RRID:AB_1079382
Rabbit polyclonal anti-TIP60	Abcam	Cat#Ab23886; RRID:AB_778485
Mouse monoclonal anti-phospho-Ser/Thr-Pro	Merck Millipore	Cat#05-368; RRID:AB_309698
Mouse anti-Beta-Tubulin	Huabio Hangzhou	Cat#M1305-2
Mouse monoclonal anti-HA	Biologend	Cat#16B12; RRID:AB_291262
Mouse monoclonal anti-Flag	ORIGENE	Cat#TA50011; RRID:AB_2622345
Goat anti-Mouse IgG (H+L), Alexa Fluor 546	Thermo Fisher Scientific	Cat#A-11003; RRID:AB_2534071
Goat anti-Rabbit IgG (H+L), Alexa Fluor 546	Thermo Fisher Scientific	Cat#A-11010; RRID:AB_2534077
Goat anti-Rabbit IgG (H+L), Alexa Fluor 405	Thermo Fisher Scientific	Cat#A-31556; RRID:AB_221605
Anti-Flag Affinity Gel	Bimake	Cat# B23102
Anti-HA Affinity Gel	Bimake	Cat# B26202
Protein A/G Agarose Resin	YEASEN	Cat# 36404ES08

(Continued on next page)

Continued

REAGENT or RESOURCE	SOURCE	IDENTIFIER
Bacterial and Virus Strains		
<i>E. coli</i> DH5a	ATCC	Cat# PTA-8019
Rosetta (DE3)	Tiagen Biotech	Cat# CB108
AAV-mCherry-GFP-LC3	Vigene biosciences	This paper
AAV-Vector	Vigene biosciences	This paper
AAV-Pacer ^{WT} -HA	Vigene biosciences	This paper
AAV-Pacer ^{2KR} -HA	Vigene biosciences	This paper
AAV-Pacer ^{S157A} -HA	Vigene biosciences	This paper
AAV-Pacer ^{S157D} -HA	Vigene biosciences	This paper
Chemicals, Peptides, and Recombinant Proteins		
Trichostatin A (TSA)	Selleck Chemicals	Cat# S1045,58880-19-6
Nicotinamide (Vitamin B3)	Selleck Chemicals	Cat# S1899,98-92-0
SB216763	Selleck Chemicals	Cat# S1075,280744-09-4
Torin1	Selleck Chemicals	Cat# S2827, 222998-36-8
Rapamycin	Selleck Chemicals	Cat# S1039,53123-88-9
KU0063794	Selleck Chemicals	Cat# S1226,938440-64-3
Leupeptin	Selleck Chemicals	Cat# S7380,103476-89-7
Bafilomycin A1	Selleck Chemicals	Cat# S1413, 88899-55-2
Acetyl-coenzyme A	Sigma	Cat# CA2056
Oil Red O	Sigma	Cat#O0625
γ - ³² P-ATP	PerkinElmer	Cat# NEG502A
Lipofectamine 2000	Invitrogen	Cat# 11668019
TRIZOL reagent	Invitrogen	Cat# 15596026
DAPI	Beyotime	Cat#C1002
Phosphatase Inhibitor Cocktail (100X)	Selleck Chemicals	Cat# B15001
Protease Inhibitor Cocktail (100X)	Selleck Chemicals	Cat# B14001
Recombinant mTORC1	Sigma	Cat# SRP0364
mTOR assay buffer	Thermo Fisher Scientific	Cat# PV4794
BODIPY493/503	Thermo Fisher Scientific	Cat# D3922
Earle's Balanced Salt Solution (EBSS)	Thermo Fisher Scientific	Cat#24010043
Pacer peptide: CGILATS(p)PYPETD	Huabio Hangzhou	phosphor-Pacer S157 polyclone antibody
Pacer full-length recombinant proteins	Purified from <i>E. Coil</i>	Anti-Pacer polyclone antibod
Critical Commercial Assays		
EnzyChrom Triglyceride Assay Kit	BioAssay Systems	Cat# ETGA-200y
EnzyChrom Ketone body Assay Kit	BioAssay Systems	Cat# EKBD-100
Deposited Data		
Original images were deposited to Mendeley data	This paper	https://data.mendeley.com/datasets/2b55j35mm6/2
Experimental Models: Cell Lines		
U2OS	ATCC	ATCC HTB-96
HEK293T	ATCC	ATCC CRL-321
LO2 (immortal hepatic cell line)	Cellbank of China	HL-7702
Experimental Models: Organisms/Strains		
Female C57BL/6 mice	Vital River, Beijing, China	N/A
Pacer Floxp/Floxp mice	CasGene, Beijing, China	N/A
B6.Cg-Tg(Alb-Cre)21Mgn/J	The Jackson Laboratory	003574

(Continued on next page)

Continued

REAGENT or RESOURCE	SOURCE	IDENTIFIER
Oligonucleotides		
Control shRNA plasmids	Sigma	SHC005
Pacer lentivirus shRNA plasmids 1	Sigma	TRCN0000141751
Pacer lentivirus shRNA plasmids 2	Sigma	TRCN0000142340
TIP60 shRNA1: GAGAAAGAATCAACGGAAG	This paper	N/A
TIP60 shRNA2: TCGAATTGTTTGGGCACTGAT	This paper	N/A
Raptor shRNA1: GATGAGGCTGATCTTACAG	This paper	N/A
Raptor shRNA2: ATCCTTAGCTCAGAGCTGG	This paper	N/A
Rictor shRNA1: CCTAATGAATATGGCTGCATCC	This paper	N/A
Rictor shRNA2: ACTTGTGAAGAATCGTATC	This paper	N/A
GSK3 α shRNA: GCTCCCAAGAAGTGGCTTA	This paper	N/A
GSK3 β shRNA: GCTAGATCACTGTAACATA	This paper	N/A
Control siRNA: UUCUCCGAACGUGUCACGUTT	GenePharma, Shanghai, China	N/A
Pacer siRNA1: GUGUUUAAGCACAGGGCUGAUTT	GenePharma, Shanghai, China	N/A
Pacer siRNA2: CAGGGCUGAUAGUUGTGGUUUTT	GenePharma, Shanghai, China	N/A
PCAF siRNA: GCAGAUACCAAACAAGUUUAUTT	GenePharma, Shanghai, China	N/A
GCN5 siRNA: GCUGAACUUUGUCAGUACAATT	GenePharma, Shanghai, China	N/A
TIP60 siRNA: GAGAAAGAAUCAACGGAAGTT	GenePharma, Shanghai, China	N/A
P300 siRNA: CUAGAGACACCUUGUAGUATT	GenePharma, Shanghai, China	N/A
CBP siRNA: AAUCCACAGUACCGAGAAUUGTT	GenePharma, Shanghai, China	N/A
ATG5 siRNA: CCUUUGGCCUUAAGAAGAAATT	GenePharma, Shanghai, China	N/A
ATG7 siRNA: AUCAGUGGAUCUAAAUCUCAATT	GenePharma, Shanghai, China	N/A
5'-DIG-TTCTACATCAGCGGGCAGCA TGAAC GTC-DIG-3'	Servicebio, Shanghai, China	Pacer CKO mouse probe <i>in situ</i> hybridization
Recombinant DNA		
pCDNA5-Pacer-3*Flag	This paper	N/A
pCDNA3.1-Pacer-HA	This paper	N/A
pEGFP-N1-Pacer	This paper	N/A
pEGFP-N1-Pacer(S157A)	This paper	N/A
pEGFP-N1-Pacer(S157D)	This paper	N/A
pCDNA5-Pacer(S157A)-3*Flag	This paper	N/A
pCDNA5-Pacer(S157D)-3*Flag	This paper	N/A
pCDNA5-Pacer(K483R)-3*Flag	This paper	N/A
pCDNA5-Pacer(K523R)-3*Flag	This paper	N/A
pCDNA5-Pacer(K533R)-3*Flag	This paper	N/A
pCDNA5-Pacer(K573R)-3*Flag	This paper	N/A
pCDNA5-Pacer(K633R)-3*Flag	This paper	N/A
pCDNA5-Pacer(5KR)-3*Flag	This paper	N/A
pCDNA5-Pacer(2KR)-3*Flag	This paper	N/A
pAV-FH	Vigene biosciences	AV88001
pAV-FH-Pacer-HA	This paper	N/A
pAV-FH-Pacer(2KR)-HA	This paper	N/A
pAV-FH-Pacer(S1571A)-HA	This paper	N/A
pAV-FH-Pacer(S157D)-HA	This paper	N/A
pCDNA5-Pacer(1-100)-3*Flag	This paper	N/A
pCDNA5-Pacer(100-300)-3*Flag	This paper	N/A
pCDNA5-Pacer(Δ 101-300)-3*Flag	This paper	N/A
pCDNA4-mLST8-myc	Donated by Jiahuai Han(cDNA)	N/A

(Continued on next page)

Continued

REAGENT or RESOURCE	SOURCE	IDENTIFIER
mTOR(rat)-myc	This paper	N/A
Raptor-myc	This paper	N/A
pCDNA3.1-PCAF-HA	Donated by Ting Liu(cDNA)	N/A
pCDNA3.1-TIP60-HA	Donated by Wei Liu	N/A
pCDNA3.1-TIP60(S86A)-HA	This paper	N/A
pCDNA3.1-P300-HA	Donated by Shimin Zhao	N/A
pCDNA3.1-CBP-HA	Donated by Jimin Shao	N/A
pCDNA3.1-GCN5-HA	Donated by Ting Liu (cDNA)	N/A
Software and Algorithms		
ZEN2	ZEISS	N/A
DNA STAR sequence assay	https://www.dnastar.com	N/A
SPSS 17 Measurement data analysis	IBM company	N/A
Image-pro-plus	http://www.mediacy.com	N/A

CONTACT FOR REAGENT AND RESOURCE SHARING

Further information and requests for reagents may be directed to and will be fulfilled by the corresponding author, Qiming Sun (qmsun@zju.edu.cn).

EXPERIMENTAL MODEL AND SUBJECT DETAILS

Cell culture

Human embryonic kidney cells HEK293T (sex unknown), human osteosarcoma cells U2OS (female), and human Liver Cell LO2 (male) were cultured in DMEM supplemented with 10% FBS, 2 mM L-glutamine, and 100U/ml penicillin-streptomycin in a humidified incubator at 37°C with 5% CO₂. HEK293T Pacer-Flag cells, HEK293T Pacer-HA cells, HEK293T GFP-LC3 cells and HEK293T control cells were obtained by lentivirus infection.

Pacer knockout mouse models

All animal experiments were performed under the guidelines of the institutional Animal Care and Use Committee at Zhejiang University. Mice were maintained in a barrier facility, at normal room temperatures, on a regular 12-h light and 12-h dark cycle. Pacer knockout mice was generated by CRISPR/Cas9 technology. Briefly, the targeting vector contained 5'-arm-Loxp-Pacer intron 3-Loxp-3'-arm cassette was constructed and the linearized construct plus pX330-sgRNA was electroporated into ESCs. Correctly targeted ESC clones were microinjected into C57BL/6 blastocysts to generate chimeric mice. The resulting progenies were backcrossed to C57BL/6J to generate Pacer flox/+mice, which were intercrossed to generate Pacer flox/flox (Pacer f/f) mice. To delete Pacer in liver, we cross Pacer f/f mice to Alb-Cre mice (Model Animal Research Center of Nanjing University, Nanjing, China), which express Cre recombinase under the control of the albumin promoter. For PCR Genotyping, genomic DNA was isolated from mouse tails and amplified by standard PCR. For the conditional knockout mice, forward primer: TTCTAACCCAGCAGGCTACGA, reverse primer: CACACCGTGCCTGAAGACTTC were used to detect both 419 bp and 462 bp product for Pacer + and Pacer flox allele, respectively. Alb-Cre transgene was amplified by forward primer (TGGCAAACATACGCAAGGG) and reverse primer (CGGCAAACG GACAGAAGCA) to obtain a specific 450 bp product.

Non-alcoholic fatty liver disease mouse model

For non-alcoholic fatty liver disease (NAFLD) mouse model, eight-week-old male C57BL/6J mice were fed for 16 weeks a freely available sterilized HFD containing 42% of the total calories from fat (TP26300, the components are the same as TD88137). **In control group, the mice received normal diet for 3 months.** After 3 months, 30 NAFLD mice were randomly divided into model group, Pacer^{WT} group and Pacer^{2KR} group. Mice in Pacer^{WT} group or Pacer^{2KR} group were **administered AAV-Pacer^{WT} or AAV-Pacer 2KR (1 × 10¹¹ cfu) in normal saline (intraperitoneal injection) and then fed for 4 weeks.** Mice in control group and model group were administered **AAV-Vector (1 × 10¹¹ cfu) in normal saline (intraperitoneal injection) and then fed for 4 weeks.**

Mouse Models of Pacer or mutant overexpression and treatment

Six-week-old female C57BL/6J mice were acclimated to handling and individual housing in standard shoebox cages in controlled conditions of a 12:12 h light: dark cycle at an ambient temperature. **For investigating the role of Pacer Phosphorylation and**

acetylation in regulating autophagy *in vivo*, recombinant adeno-associated virus packing Pacer^{WT}, Pacer^{S157A}, Pacer^{S157D} and Pacer^{2KR} vectors were produced in HEK293T cells (Vigenebio, China). Mice were intraperitoneally injected with the control virus, Pacer^{WT}, Pacer^{S157A}, Pacer^{S157D} or Pacer^{2KR} (1×10^{11} cfu). Four weeks after viral injection, the half of mice in each group were injected 40 mg/kg leupeptin into the peritoneal cavity. The mice were treated for 12 h and sacrificed for the analysis of autophagy level by p62 degradation.

METHOD DETAILS

p62 degradation assay

HEK293T cells were transiently transfected with Pacer mutants and were treated with EBSS medium for 1 h in the presence or absence of Baf A1. The whole cells lysates were briefly sonicated in 1 × SDS loading buffer and incubated at 100°C for 5 min, then subjected to western blot analysis with antibodies against p62.

Autophagosome maturation assay

Pacer knockdown U2OS cells were infected with AAV GFP-mCherry-LC3. After 24 h post-infection, the cells were transfected with resistance Pacer mutants and LC3 puncta was analyzed by fluorescence microscopy.

Immunoprecipitation and western blot

Cells for protein analysis were homogenized in TAP buffer (20mM Tris-HCl, pH 7.4, 150mM NaCl, 0.5% NP-40, 1mM NaF, 1mM Na₃VO₄, 1mM EDTA, 10nM MG132, supplemented with protease and phosphatase inhibitors) for 30 min at 4°C. For acetylation immunoprecipitation, 2 μM TSA and 10mM NAM were added. The cell lysates were centrifuged at 14,000 rpm for 15 min, and the supernatants were incubated with antibody-conjugated beads and rotated for 4 h at 4°C, then the beads were washed three times with TAP buffer and eluted with 1 × SDS loading buffer. Samples were separated with SDS-PAGE, transferred to Polyvinylidene Fluoride Membrane and probed with the corresponding antibody.

Immunofluorescence

For protein colocalization assay, cells transfected with different plasmids were plated on coverslips, fixed with 4% paraformaldehyde in PBS for 20 min at room temperature and permeabilized with 0.1% Triton X-100 in PBS for another 20 min. Cells were blocked in blocking buffer (1% BSA, 0.1% Triton X-100 in PBS) for 1 h, then stained with primary antibodies diluted in blocking buffer overnight at 4°C, and washed with PBS three times. After that, the cells were then stained with corresponding Alexa Fluor-conjugated secondary antibodies in blocking buffer for 1 h at room temperature and washed with PBS three times. Slides were mounted and imaged with a laser scanning confocal microscope (Zeiss LSM 800). For lipid droplets staining, cells were fixed with 4% paraformaldehyde in PBS for 20 min at room temperature and wash 3 times in PBS. After that, the cells were then stained with BODIPY493/503 in blocking buffer for 1 h at room temperature.

Transmission electron microscopy

U2OS cells that transiently transfected with recombinant vectors in control cells or Pacer KD cells and liver tissues from mouse model were fixed in 2.5% glutaraldehyde in PBS overnight at 4°C and washed three times for 15 min with 0.1M phosphate buffer, and then fixed in 2% aqueous osmium tetroxide for 1 h followed by washing three times each for 15 min with deionized water. Samples were then dyed with 2% uranyl acetate for 30 min, and dehydrated through graded alcohols (50%–100%) and 100% acetone each for 15 min. After that, Samples were embedded in EPON 812 resin and cured for 24 h at 37°C, 45°C, 60°C, respectively. Ultrathin (70 nm) sections were obtained by ultra-thin slicer machine and stained with 2% uranyl acetate and 0.3% lead citrate. Electron microscopy images of the samples were taken using Tecnai G2 Spirit transmission electron microscope (FEI Company).

In vitro acetylation assay

In vitro acetylation assays were performed in 30 μL of reaction mixture containing 20 mM Tris-Cl, pH 8.0, 20% glycerol, 100 mM KCl, 1 mM DTT and 0.2 mM EDTA, 10 μM TSA, 10mM nicotinamide, 100 μM acetyl-CoA, TIP60-HA (purified from HEK293T) and 1 mg Pacer-Flag. After incubation at 30°C for 1 h, the reaction was stopped by addition of 10 μL of 5 × SDS sample buffer. The samples were subjected to SDS-PAGE and visualized by silver staining. Specific bands were cut off and subjected to mass spectrometry analysis (AIMS scientific Co., Ltd, Shanghai, China) or western blot.

In vitro kinase assay

In vitro kinase assay was performed as described previously (Yu et al., 2011). Briefly, purified recombinant Pacer-Flag was incubated with mTORC1 in 50 μL of reaction mixture containing 10 μM ATP, 10 μg Pacer-Flag, 250 ng mTORC1, 2mM DTT, protease inhibitors, and 1 × mTORC1 kinase buffer. After incubated at 37°C for 30 min, the reaction was terminated by the addition of 15μL of 5 × SDS loading buffer. The samples were then subjected to SDS-PAGE and visualized by silver staining. Specific bands were cut off and subjected to mass spectrometry analysis (AIMS scientific Co., Ltd, Shanghai, China).

Triglyceride content in liver and cultured hepatocytes

For tissues, liver (250 mg) was homogenized in 1 mL of methanol/ chloroform (1:2, v/v), followed by shaking at room temperature for 2 h and centrifuged at 12000 rpm for 10 min. Then 150 μ L of the organic phase was transferred to a new tube and air-dried in a fume hood overnight at room temperature. The original lipid extract was resuspended in 5% Triton X-100 at room temperature for 1 h. The triglyceride level was determined using the EnzyChrom triglyceride assay kit (Bioassay Systems). For cells, LO2 cells were treated with different way. 1×10^5 cells can be solubilized in 40 μ L 5% Triton X-100 for 30 min. The cell lysates were centrifuged at 14,000 rpm for 15 min and the supernatant was transferred to a new centrifuge tube. Transfer 10 μ L samples into separate wells of the 96-well plate. The triglyceride level was determined using the EnzyChrom triglyceride assay kit (Bioassay Systems).

Ketone body assay in serum and liver tissues

Serum were obtained from peripheral blood in Pacer f/f and Pacer f/f; Alb-Cre mice under fed or fasting for 24 h. For liver tissues, liver (100 mg) was homogenized in 100 μ L PBS containing 0.5% NP-40, and then cell lysate was centrifuged at 12000 rpm for 30 min. The serum and liver supernatants used to determine ketone body containing acetoacetic acid (AcAc) and 3-hydroxybutyric acid (BOH). Total ketone body concentration is calculated as [Total ketone body] = [AcAc] + [BOH]. AcAc and BOH were measured according to the manufacturer's protocols of EnzyChrom ketone body assay kit (Bioassay Systems).

Protein extraction from tissue

Liver or heart samples(200 mg)were homogenized in 1 mL TAP buffer (20 mM Tris-HCl, pH 7.4, 150 mM NaCl, 0.5% NP-40, 1 mM NaF, 1 mM Na_3VO_4 , 1 mM EDTA, 10 nM MG132, supplemented with protease, phosphatase inhibitors, and deacetylase inhibitors) using an homogenizer at 4°C for 45 s, and the homogenates were cleared by centrifugation at 14,000 rpm for 20 min and 200,000 g for 60 min, respectively. The supernatants were used for western blot analysis or immunoprecipitation.

Fractionation by differential centrifugation

HEK293T cells that were transiently transfected with Pacer^{WT}-Flag, Pacer^{S157A}-Flag and Pacer^{S157D}-Flag for 24 h were treated with EBSS medium for 1 h. The cells were harvested by centrifugation at 1,000 rpm for 10 min. The cell pellets were washed with PBS and centrifuged at 1,000 rpm for 10 min. The cells were suspended in 5 \times volume of buffer A (20 mM HEPES, pH 7.4, 40 mM KCl, 1.5 mM MgCl_2 , 1 mM EDTA, 1 mM EGTA, 0.1 mM PMSF, 10% Glycerol and 250 mM sucrose) and incubated on ice for 30 min. The cells were homogenized by passing through a 22G needle 24 times. After centrifugation at 1,000 g for 10 min, the supernatant was harvested and subjected to centrifugation at 100,000 g for 0.5 h. The supernatant was designated as S100 and the pellet was designated as P100. S100 and P100 were dissolved with 1xSDS loading buffer and were subjected to western blot to analysis Pacer mutant and TIP60.

RNA Isolation and qPCR Analyses

Total RNA was isolated using Trizol reagent (Invitrogen). 1.0 μ g of the total RNA was reverse transcribed into cDNA, using the HiScript II 1st Strand cDNA Synthesis Kit. Quantitative real-time PCR analysis was performed using HiScript II Q Select RT SuperMix for qPCR and real-time PCR machine (CFX-96, Bio-Rad). The relative mRNA expression levels of p62, Tip60, MYST1, MYST2, MYST3 and MYST4 were calculated from the corresponding standard curve by the indicated software and normalized with the β -actin level in the same sample.

Oil red O staining

The magnitude of liver lipid accumulation was measured by Oil Red O (ORO) staining. Liver tissues were fixed in ice-cold 4% (w/v) paraformaldehyde for 24 h. Liver sections were washed twice with PBS, stained with Oil Red O solution, differentiated with 50% ethanol, rinsed with tap water and finally counterstained with hematoxylin. The sections were photographed and analyzed by microscope (Olympus Corporation).

Hematoxylin and Eosin Staining and Immunohistochemistry

Hematoxylin (HE) staining was performed to analyze histopathologic changes of liver according to standard protocols. Immunohistochemistry (IHC) was performed to analyze Pacer and p62 protein expression in liver. Briefly, IHC was used on 4 μ m sections taken from ice-cold 4% (w/v) paraformaldehyde fixed paraffin embedded tissue. Sections were mounted on microscope slides and heated at 60°C for 1 h to attach the sections to the slide. Sections were deparaffinized in three changes of xylene and rehydrated through graded concentrations of ethanol. For immunostaining, deparaffinized and rehydrated sections were heated in citrate buffer at 121°C for 30 min to retrieve antigenic activity. Endogenous peroxidase activity was inhibited by incubation with 0.3% hydrogen peroxide in methanol for 20 min. After nonspecific reactions had been blocked with 10% normal bovine serum, the sections were incubated with rabbit polyclonal antibodies specific to Pacer (1:100; homemade) at 4°C overnight and then with horseradish peroxidase-conjugated secondary antibody at 37°C for 1 h. The sections were counterstained with hematoxylin for detection.

***In situ* hybridization**

Deparaffinized and rehydrated sections were prewarmed in TPBS containing proteinase K solution in TPBS (20 μ g/mL) and agitated at 37°C for 25 min and then wash briefly with PBS buffer. Endogenous peroxidase activity was inhibited by incubation with 0.3% hydrogen peroxide in methanol for 20 min. The sections were incubated prewarmed 56°C prehybridization buffer for 1 h at 56°C in the hybridization oven. Preheat the diluted probes at 80°C for 10 min in a heating block. Quickly exchange the prehybridization solution with the diluted probe solution to avoid cooling of the latter and incubate the sections in this solution at 56°C for 16–20 h. The sections were blocked by 5% BSA and then incubated with mouse anti-DIG-HRP at 37°C for 40 min. Finally, sections were developed in 3,3'-diaminobenzidine (DAB) solution and mounted by neutral balata.

QUANTIFICATION AND STATISTICAL ANALYSIS

All experiments were independently repeated at least three times. The sample size was chosen according to the well-established rules in the field. Statistical analyses were performed using the two-tailed Student's *t* test. Values are expressed as mean \pm SD of at least three independent experiments, unless otherwise noted. "n" represents mouse number in [Figures 1, S1, 7, and S7](#). "n" represents experimental replication in [Figures 3E, 4I, 6C, S4C, S4E, S5I, S5J, S6B, and S6H](#). "n" represents cell micrographs in [Figures 3G, 5D, 6G, S3B, S3E, and S6D](#). The levels of significance of 0.05 (*), 0.01 (**), and 0.001 (***) or lower were considered statistically significant.